Astrocytic Microdomains Confine A “molecular Memory” Enabling Long-Term Information Storage for Memory Consolidation

Beatrice Vignoli
University of Trento
Gabriele Sansevero
University of Florence
Manju Sasi
University Hospital Würzburg
Roberto Rimondini-Giorgini
University of Bologna
Robert Blum
University Hospital Würzburg
Spartaco Santi
National Research Council of Italy/IRCCS https://orcid.org/0000-0001-9856-7053
Nicoletta Berardi
University of Florence
Bai Lu
Tsinghua University
Marco Canossa (marco.canossa@unitn.it)
University of Trento

Article

Keywords: astrocytic, microdomains, molecular

Posted Date: January 28th, 2021

DOI: https://doi.org/10.21203/rs.3.rs-139639/v1

Version of Record: A version of this preprint was published at Communications Biology on October 5th, 2021. See the published version at https://doi.org/10.1038/s42003-021-02678-x.

Astrocytic microdomains confine a "molecular memory" enabling long-term information storage for memory consolidation

Beatrice Vignoli,[1*] Gabriele Sansevero, [2] Manju Sasi,[3] Roberto Rimondini-Giorgini,[4] Robert Blum,[3] Spartaco Santi,[5] Nicoletta Berardi,[6] Bai Lu,[7] Marco Canossa [8,*]

[1] Department of Physics/Nanoscience Laboratory/Department of Cellular, Computational and Integrative Biology (CIBIO) University of Trento, Povo (TN), 38123, Italy.

[2] Department of Neuroscience, Psychology, Drug Research, Child Health (NEUROFARBA), University of Florence, Florence, 50100, Italy/IRCCS Stella Maris Foundation, 56128 Pisa, Italy.

[3] Institute of Clinical Neurobiology, University Hospital Würzburg, Würzburg, 97078, Germany.

[4] Department of Medical and Surgical Sciences (DIMEC), University of Bologna, Bologna, 40126, Italy.

[5] Institute of Molecular Genetics "Luigi Luca Cavalli-Sforza", National Research Council of Italy/IRCCS, Istituto Ortopedico Rizzoli, Bologna, 40136, Italy.

[6] Department of Neuroscience, Psychology, Drug Research, Child Health (NEUROFARBA), University of Florence, Florence, 50100, Italy.

[7] School of Pharmaceutical Sciences, Tsinghua University, Beijing, 100084, China.

[8] Department of Cellular, Computational and Integrative Biology (CIBIO) University of Trento, Povo (TN), 38123, Italy.

* Correspondence: marco.canossa@unitn.it; beatrice.vignoli@unitn.it

Abstract

Memory consolidation requires astrocytic microdomains for protein recycling; but whether this lays a mechanistic foundation for long-term information storage remains enigmatic. Here we demonstrate that persistent synaptic strengthening invited astrocytic microdomains to convert initially internalized (pro)-brain-derived neurotrophic factor (proBDNF) into active prodomain (BDNFpro) and mature BDNF (mBDNF) for synaptic re-use. While mBDNF activates TrkB, we uncovered a previously unsuspected function for the cleaved BDNFpro, which increases TrkB/SorCS2 receptor complex at post-synaptic sites. Astrocytic BDNFpro release reinforced TrkB phosphorylation to sustain long-term synaptic potentiation and to retain memory in the novel object recognition behavioral test. Thus, the switch from one inactive state to a multi-functional one of the proBDNF provides post-synaptic changes that survive the initial activation (molecular memory). This molecular asset confines local information storage in astrocytic microdomains to selectively support memory circuits.

Introduction

The most intriguing aspect of long-term potentiation (LTP) is the molecular basis essential for its persistence, a suggestive hallmark for memory consolidation. Crick first tackled the hypothesis that long-term memory storage is centered on a self-sustained molecular adaptation, suggesting protein phosphorylation as a paradigm (1). Later on, the discovery of in-side activation of CaMKII (2), confirmed the existence of ‘‘memory molecules”. CaMKII is initially activated by Ca^{2+}-Calmodulin. Due to a mechanism of self-phosphorylation that makes the enzyme constitutively active, CaMKII no longer requires the presence of Ca^{2+}-Calmodulin for its functionality (3, 4). More recently, Kandel and co-workers reported on a different process by showing that prion-like proteins (CPEB), aggregated in a self-perpetrating state are involved in the stabilization of long-lasting synaptic changes through the control of local protein synthesis (5). Thus, a variety of proteins that no longer experiences the initial activation can maintain memory. In line with this rather simple but attractive model, the mechanism that converts a transient neuronal stimulation into a persistent synaptic signaling during LTP has been a long-standing question (6).

Neurons are exquisitely specialized for rapid electrical transmission of signals, but glial cells, which do not communicate with electrical impulses are ideal for participating in cognitive functions requiring long-term temporal regulation and broad spatial integration (7–9). In the present study, we report that astrocytic membrane protrusions enwrapping synaptic terminals (microdomains) are a previously unsuspected synaptic compartment for the confinement of a “molecular memory”. Once stimulated, neurons serve synthesis and release of brain-derived neurotrophic factor (BDNF) into the extracellular space (10), a key step in the induction of long-term synaptic modification (11). In addition, neurons provide secretion of the precursor protein (~32 kDa proBDNF), consisting of prodomain (~12 kDa BDNFpro) and mature protein (~14 kDa mBDNF) (12). We have previously reported that proBDNF is cleared by astrocytic microdomains *via* $p75^{NTR}$-mediated endocytosis (13–15) and recycled back to neurons for LTP stabilization and memory retention (15). Here we demonstrated that astrocytic microdomains coordinate in subsequent steps, (i) the processing of previously internalized proBDNF to generate

BDNFpro and mBDNF products; (ii) the vesicular storage and (iii) secretion of the proteolytic products for synaptic re-use. While mBDNF commonly activate TrkB, astrocytic release of BDNFpro increases TrkB expression at the spines surface, which captures sufficient neurotrophin signaling for LTP maintenance. Hence, the persistence in synaptic strength is due to both an additional supply of mBDNF from astrocytic microdomains and to an increase in the post-synaptic response to neurotrophin by the prodomain. Astrocytic release of BDNFpro, ultimately provides the molecular basis for retaining memory in the novel object recognition behavioral test. Thus, neurons and glia are associated by neurotrophins in functional memory units, which build reinforcing cellular and molecular loops enabling a persistent strengthening of the synapse and memory consolidation.

Results

proBDNF processing in astrocytes

Protoplasmic astrocytes are one type of morphologically characterized glial cells. Cortical layer II/III astrocytes show a highly branched arborization and fine membrane extensions in the cell periphery that enwraps synaptic contacts (16). We have previously reported that cortical layer II/III astrocytes support clearing and recycling of proBDNF (13, 15, 17) to sustain TrkB signaling and LTP maintenance in perirhinal cortex (15). However, neither TrkB phosphorylation (18) nor the late-phase LTP (19, 20) are directly regulated by proBDNF, suggesting that conversion of the inactive neurotrophin precursor to an active product might play a more direct role. We now ask whether these same astrocytes are proficient for direct cleavage of endocytic proBDNF following LTP-inducing electrical stimulation.

Brain slices of control mice were prepared to examine the astrocytic origin of the proBDNF processing. Their perirhinal cortex was previously injected in layer II/III with adenoviral particles transducing green fluorescent protein (GFP) under the regulation of glial fibrillary acidic protein (GFAP) promoter (AAV-GFAP-GFP) (21). Furthermore, in order to avoid the injection procedure, transgenic mice stably expressing GFP under the control of GFAP promoter (GFAP-GFP mice) (22) have been used. Slices were used for field stimulation delivering θ-burst-stimulation (TBS) evoking LTP (23). The occurrence of proBDNF proteolytic processing was analyzed 10 min after stimulation by immunohistochemistry using an antibody (αBDNFpro) that specifically recognizes the furin cleaved C-terminal end of the prodomain (Fig. 1a; (24)). This epitope is unavailable in both intact proBDNF and mBDNF, providing that the antibody recognized the cleaved BDNFpro, leaving undetected cleavage-resistant proBDNF (proBDNF^{CR}) and mBDNF in the Western blot analysis (Fig. 1a). BDNFpro and GFP immunoreactivity was analyzed by confocal microscopy to appreciate the specific distribution of the cleaved prodomain in individual astrocytes (Fig. 1b and Supplementary Fig. 1a). GFP is a cytosolic protein whose fluorescence defines the astrocyte in its entire cytoplasmic extension. This is a feature that is ideal to achieve detection of BDNFpro in the astrocytic territorial volume. Spatial overlap of BDNFpro and GFP was analyzed in a series of confocal stacks by

using colocalization analysis of the two signals (Supplementary Fig. 1c). To facilitate BDNFpro visualization in the astrocytic territorial volume, BDNFpro/GFP colocalization was reconstructed in z-stacks. We observed sharp BDNFpro/GFP colocalization signal, as detected by αBDNFpro, in astrocytes from TBS-slices (Fig. 1c and Supplementary Fig. 1b). Cleaved prodomain detection was observed in small proportion at the cell body and in greater proportion in the cell periphery mostly matching with highly ramified processes. In marked contrast, basal stimulation induced little BDNFpro/GFP colocalization signal in astrocytes (Fig. 1c and Supplementary Fig. 1b). For quantification analysis, we used Mander's overlap and measured the extent of co-occurrence (25) between the two fluorophores. By this analytical parameter, the proportion of BDNFpro/GFP colocalization was increased in the whole cell (Fig. 1c and Supplementary Fig. 1b) or branches subcellular regions (Fig. 1c) in TBS vs. basal conditions. Additional colocalization parameter as the Pearson's correlation was used (Supplementary Fig. 1d), confirming that in TBS-slices BDNFpro/GFP colocalization signal significantly increased over baseline.

Glial cells were reported to lack de novo proBDNF synthesis under physiological conditions (26), suggesting that BDNFpro detection in these cells originates from the proBDNF that was previously endocytosed and then cleaved. Preventing proBDNF internalization in astrocytes would then prevent the precursor processing and accordingly BDNFpro detection. This assumption was validated by experiments conducted in loxP-$p75^{NTR}$-loxP mice (27) crossed with GLST-$CreER^{T2}$ (28) and Rosa-CAGloxP-stop-loxP(LSL)-R26R mice (29); for simplicity p75-flox mice (Supplementary Fig. 2a; (30)). Tamoxifen administration by intraperitoneal injection into adult p75-flox mice induced $p75^{NTR}$ gene deletion, the carrier receptor for proBDNF uptake in these cells (15), and expression of β-Galactosidase (β-Gal) reporter. Virtually, all β-Gal+ cells in the cortex showed the morphology of protoplasmic astrocytes (Supplementary Fig. 2b) and the vast majority of them were GFAP+ (81 ± 4%). Conversely, very few β-Gal+ cells expressed NeuN-neuronal marker (1 ± 0.7%), demonstrating that p75-flox mice allowed astrocytes selective targeting in the brain cortex in vivo. Immunoreactivity for BDNFpro was examined in slices from p75-flox mice 14 days post-tamoxifen (dptm). This latency

ensured a significant depletion of $p75^{NTR}$ protein following recombination in astrocytes (Supplementary Fig. 2c). In $p75^{NTR}$-deficient cells, BDNFpro/GFP signal was hardly detectable in both TBS and basal stimulation (Fig. 1d). Thus, $p75^{NTR}$-mediated proBDNF endocytosis fed astrocytes with a cleavable pool of proBDNF.

Collectively, our data indicate that proBDNF is a substrate for proteolytic processing in cortical layer II/III astrocytes following LTP-mediated internalization. Given that endocytic proBDNF undergoes recycling in this potentiating condition (15), our data suggest that astrocytes might convert proBDNF into BDNFpro and mBDNF at peri-synaptic sites before routing to the secretory pathway.

Localization of BDNFpro in astrocytic microdomains

The intricate ramifications of astrocytes allow them to tightly enwrap the synaptic terminals at organized peri-synaptic structures, the microdomains (31). Astrocytic microdomains can be distinguished into *thick* processes of micrometer scale (~10-15 μm^2) that host endoplasmic reticulum (ER) and mitochondria capable of generating inositol-3-phosphate (IP3)-dependent Ca^{2+} signals and *thin* organelle-free structures of submicron/nanometer-scale that fill the space between synapses (32–34). We speculated that astrocytic proBDNF processing might be achieved on a rapid time scale at microdomains and, possibly, within the same storage compartments orchestrating the recycling process. Vesicular localization of the cleaved BDNFpro targeting astrocytic microdomains has been evaluated to be in line with our hypothesis.

Subcellular localization of BDNFpro was initially resolved in super-resolution by using structured illumination microscopy (SIM) (Fig. 2a). In TBS-slices from control mice, BDNFpro/GFP colocalization signal appeared as a punctate pattern dispersed into cell periphery of astrocytes. At higher magnification, BDNFpro/GFP colocalization was present in membrane ramifications mostly shaped as finger-like extensions and flat lamellar sheaths (Fig. 2a, b), which were recognized to be astrocytic structures contacting the synapse. Quantification analysis confirmed that TBS induced a significant increase of the colocalization signal (45 ± 6% of the total BDNFpro/GFP puncta detected in astrocytes) in these specific structures. Given the nanometer scale resolution of the SIM

super-resolution microscopy (lateral res. 115 nm; axial res. 250 nm), our data suggest for an enrichment of the cleaved prodomain in high membranous elaborations of the cell periphery viewing the dimensions and typical morphology of microdomains.

To firmly assess this conclusion, we extended our investigation at ultra-structural levels (15). Ultra-thin sections from TBS-slices were examined by transmission electron microscopy (EM) in pre-embedding experiments (Fig. 3a). At 70,000-100,000-fold magnification, immunogold labeling was observed using αBDNFpro antibody (αBDNFpro-gold) in (i) vesicular structures at pre-synaptic terminals typically displaying clouds of synaptic vesicles opposed to post-synaptic density structures (Fig. 3b); (ii) post-synaptic terminals (Fig. 3b); and (iii) astrocytes giving rise to fine astrocytic processes in close proximity to the synapses (Fig. 3c). Consistent with our data that BDNFpro in astrocytes is generated from endocytic proBDNF processing in response to neuronal activity, TBS-slices showed a higher number of αBDNFpro-gold grains in astrocytes filling the space between synapses (38 ± 7% of the total gold particles detected in astrocytes) with respect to non-stimulated slices (12 ± 4% of the total gold particles detected in astrocytes). Most gold particles were organized in groups of many grains and were concentrated peri-synaptically (46 ± 4% of the total gold particles detected in astrocytes) in a membrane-delimited area of 230 nm radius surrounding synaptic contacts (Supplementary Fig. 3a). This distance represents the maximum of the astrocyte volume fraction when astrocytes cover dendritic spines and axonal boutons (35). A similar enrichment was previously reported (15), using αmBDNF-gold (Supplementary Fig. 3b) or αproBDNF-gold (Supplementary Fig. 3c) potentially detecting both proBDNF and mBDNF isoforms or proBDNF and BDNFpro, respectively, suggesting for proBDNF processing in this area.

Lastly, we addressed the vesicular localization of BDNFpro. Endocytic proBDNF was shown to localize in vesicles expressing both $p75^{NTR}$ (13, 15) and Vamp2 (36), a component of the core SNARE complex; thus indicating that intracellular storage of endocytic proBDNF in astrocytes involves vesicles equipped with the molecular machinery deputed to both endocytosis and exocytic fusion (recycling vesicles). In line with these findings, we discovered BDNFpro/GFP colocalization that overlapped with

198 Vamp2/GFP colocalization in the astrocytic territory (Fig. 4a), suggesting that the
199 processing of the precursor takes place at recycling vesicles. Moreover, the vesicular
200 localization of the prodomain in astrocytes was analyzed by BDNFpro/Vamp2
201 colocalization using SIM super-resolution microscopy, thereby at a resolution limit
202 compatible with the dimension of astrocytic microdomains. In TBS-slices,
203 BDNFpro/Vamp2 colocalization signal appeared as a punctate pattern reminiscent of
204 vesicular structures dispersed into cell periphery of astrocytes (Fig. 4b). Vesicular
205 localization of BDNFpro was further observed at ultrastructural level (Fig. 4c, d);
206 vesicles filled with BDNFpro-gold were occasionally seen at the astrocytic limiting
207 membrane near synaptic endings. Similar vesicular localization was previously reported
208 using αproBDNF-gold or αmBDNF-gold (15); however, a reliable quantification of these
209 storage organelles was inhibited by our pre-embedding procedure (15, 37). This
210 procedure resulted to a poor preservation of ultrastructural details in astrocytes, while
211 ensuring the specificity of BDNFpro signal by preserving the antibody antigenicity. We
212 conclude that vesicles containing BDNFpro are created at astrocytic microdomains in
213 response to TBS.
214
215 **Astrocytic BDNFpro is sufficient for LTP maintenance**
216 A central hypothesis arising from proBDNF processing in recycling vesicles is that the
217 resulting end products participate in gliotransmission, supplying astrocytes with a
218 releasable source of active neurotrophins and enabling LTP maintenance. Conversion of
219 proBDNF to mBDNF would typically satisfy this requirement. However, given that
220 BDNFpro and mBDNF (15) share similar vesicular localization, we formulated the
221 original hypothesis that BDNFpro individually participates to synaptic strengthening *via*
222 the recycling process.
223 To assess the contribution of BDNFpro in LTP, we performed LTP-rescue experiments in
224 conditional p75-flox mice as reported previously (15). In these experiments astrocytes are
225 incapable of proBDNF uptake, resulting in a short-lived potentiation that declined to
226 baseline about 140 min after TBS (Supplementary Fig. 4a). Conversely, expression of
227 proBDNF (Supplementary Fig. 4b), but not cleavage resistant proBDNF^{CR}

(Supplementary Fig. 4c) in astrocytes restores LTP for the 180 min duration of the recording to levels exhibited by control littermates. An ectopic source of cleavable proBDNF in $p75^{NTR}$-deficient astrocytes would then be assumed to replenish endocytic proBDNF and compensate for the lack of recycling in these cells, restoring the LTP deficits. Using this strategy, we expressed BDNFpro specifically in $p75^{NTR}$-deficient astrocytes for LTP assessment.

First, we engineered a lentiviral construct (LV-$BDNFpro^{stop}$) for BDNFpro expression (Supplementary Fig. 5a). In this construct, a loxP-GFP-STOP-loxP cassette allows GFP expression while preventing for BDNFpro expression. The GFP-STOP cassette is removed in the presence of Cre recombinase, finally resulting in GFP loss and activation of the BDNFpro transgene and Tomato reporter. We injected LV-$BDNFpro^{stop}$ into perirhinal cortices of p75-flox mice at 0 or 12 dptm. At 14 dptm (Supplementary Fig. 5b), cortical slices were prepared and stained for the astrocytic marker GFAP, the mouse reporter β-Gal and the viral reporter Tomato. Most Tomato+ cells (98 ± 4%) were recombined astrocytes (GFAP+/β-Gal+) indicating the specificity of the lentiviral construct. In addition, we found that transduced astrocytes from both injection times expressed comparable levels of BDNFpro immunoreactivity, which was in the range of the one observed in TBS-slices from control littermates (Supplementary Fig. 5c). This is consistent with the expectation that virally transduced BDNFpro replaces the prodomain generated by endocytic proBDNF processing.

In parallel, slices were used for field recordings. While basal synaptic transmission (input-output; Supplementary Fig. 5d) and synaptic facilitation (paired-pulse facilitation; Supplementary Fig. 5e) were unaffected by LV-$BDNFpro^{stop}$ transduction, slices from p75-flox mice injected with the virus showed to restore long-lasting LTP deficits (Fig. 5a and Supplementary Fig. 4d). Thus, supplying astrocytes with the sole BDNFpro expression compensates for the physiological presence of proBDNF uptake, processing, and final recycling of the proteolytic products. Prerequisite for this process is that virally transduced BDNFpro in astrocytes undergoes to secretion enabling LTP maintenance. To assess this issue, we designed a lentiviral construct for specific expression of Tetanus Toxin (TeTN) light-chain (LV-$TeTN^{stop}$) in astrocytes (Supplementary Fig. 5a).

Sustained astrocytic expression of TeTN - a protease known to cleave the SNARE protein Vamp2 (36) - is expected to inhibit the fusion of all secretory vesicles including those containing the neurotrophin (13). We injected LV-TeTN^{stop} together with LV-BDNFpro^{stop} in perirhinal cortices of p75-flox mice the last day of tamoxifen treatment (Fig. 5b). At 14 dptm, cortical slices were used for LTP recordings. Slices from double-injected mice showed LTP that decayed to baseline 120-140 min in response to TBS; while co-injecting LV-GFP^{stop} and LV-BDNFpro^{stop} viruses into the contralateral hemisphere of the same mice showed to restore the LTP deficits to the levels exhibited by control littermates. Thus, docking and fusion of Vamp2-secretory vesicles containing BDNFpro are required for LTP maintenance.

Whether BDNFpro is sufficient for rescuing LTP deficit was next investigated. Slices from p75-flox mice were perfused with exogenous BDNFpro (10 ng/ml) for 10 min (Fig. 5c). This timing was chosen as it correlates with the duration of proBDNF recycling in this cortical area (15). Exogenous application of the BDNFpro fragment initiated 2 min before TBS and was maintained for additional 8 min. We found that fEPSP was significantly restored in p75-flox mice receiving recombinant BDNFpro compared to vehicle-treated slices. Given that exogenous administration of mBDNF (10 ng/ml), but not cleavage-resistant proBDNF^{CR} (20 ng/ml), similarly rescued LTP deficits (Supplementary Fig. 6a), our data indicate that proBDNF processing provides a mechanistic link between proBDNF clearing and subsequent recycling of the converted products, both possessing same individual ability to sustain LTP. Moreover, when TBS was omitted from the paradigm, BDNFpro application had no effect on fEPSP responses over a 180 min period of baseline test-stimulation (Supplementary Fig. 6b), indicating that BDNFpro requires TBS for participating in synaptic strengthening. The rescuing effect of recombinant BDNFpro is a transient phenomenon that saturates over time, as demonstrated by applying BDNFpro for 10 min at different time points after TBS (Supplementary Fig. 6c). The period of BDNFpro dependency ended about 110 min from TBS; after this time, application of the pro-fragment could no longer restore LTP deficit. Thus, BDNFpro is required for a limited time window to sustain LTP.

Collectively, our data indicate astrocytes to be as proficient for BDNFpro release, which fulfills the function to mediate the switch from early- to late-phase LTP.

BDNFpro$^{Val/Met}$ preserves bioactivity

A single-nucleotide polymorphism in the human BDNF gene results in valine (Val) to methionine (Met) substitution at codon 66 (Val66Met) in the prodomain region causing memory alteration in humans (38, 39) and impaired synaptic strengthening in transgenic mice carrying the mutation (40). By these premises, we investigated whether structural changes induced by this amino acid substitution might compromise BDNFpro function on LTP maintenance. Slices from p75-flox mice were perfused with recombinant BDNFpro carrying the genetic variation (BDNFpro^{Val66Met}) and subjected to TBS. We found that BDNFpro^{Val66Met} (10 ng/ml) applied for 10 min in stimulated slices (Fig. 5d) retained the ability to restore LTP deficit. Thus, Val66Met substitution does not subtract bioactivity to BDNFpro in our experimental context.

Astrocytic BDNFpro increases post-synaptic TrkB signaling

BDNFpro is believed to be ligand for the sortilin family member receptor SorCS2 (41). A potential function attributed to SorCS2 is to act as co-receptor for TrkB, assisting the assembling and targeting of TrkB/SorCS2 complex to post-synaptic membranes (42). In this way, it recruits sufficient TrkB signaling for LTP maintenance. Once recycled by astrocytic microdomains, BDNFpro would then support aggregation and targeting of TrkB/SorCS2 complex at post-synaptic sites.

To assess this mechanistic issue, cultured cortical neurons expressing GFP were subjected to in situ proximity ligation assay (PLA) (42). This experimental strategy requires PCR-amplification to hybridize fluorescent DNA probes coupled to secondary antibodies (αrabbit IgG and αgoat IgG) targeting αTrkB (rabbit) and αSorCS2 (goat) primary antibodies (Fig. 6a). Hybridization takes place only when probes are localized less than 40 nm apart, which reflects TrkB/SorCS2 clustering in our experimental context. In vehicle-treated neurons, basal PLA$^{TrkB/SorCS2}$ -signal appeared as sparse fluorescent pattern (Fig. 6b). Fluorescent signal increased after treating neurons with

317 exogenous BDNFpro (10 ng/ml) for 10 min. PLA$^{TrkB/SorCS2}$ -signal was prominent in the
318 plasma membrane of both cell body and dendritic processes, indicating a clear post-
319 synaptic localization of TrkB/SorCS2 aggregates. Strikingly, PLA$^{TrkB/SorCS2}$ -signal in
320 dendrites was predominately concentrated in proximity of spines, appearing as membrane
321 protrusion extending from dendritic processes (Fig. 6b). Quantitative analysis confirmed
322 the increase of PLA$^{TrkB/SorCS2}$-signal in BDNFpro-treated vs. vehicle-treated cultures (Fig.
323 6c). The specificity of BDNFpro treatment was assessed by pre-treating neurons for 20
324 min with αSorCS2 (20 μg/ml) (Fig. 6b), a blocking antibody that is known to prevent
325 TrkB/SorCS2 complex formation (42). In the presence of αSorCS2 pre-treatment,
326 BDNFpro fragment could no more exert its aggregating effect and PLA$^{TrkB/SorCS2}$ -signal
327 could not be seen (Fig. 6c). Moreover, when neurons were treated with recombinant
328 mBDNF (10 ng/ml), or cleavage-resistant proBDNF^{CR} (20 ng/ml), PLA$^{TrkB/SorCS2}$-signal
329 had not changed significantly as compared to vehicle-treated neurons (Fig. 6c); that
330 indicates that, within BDNF isoforms, TrkB/SorCS2 aggregation is a unique function of
331 BDNFpro. PLA analysis was extended to cortical slices from control mice 10 min after
332 basal- or TBS-stimulation (Fig. 6d). We measured in a quantitative analysis,
333 PLA$^{TrkB/SorCS2}$ signal that colocalized with the postsynaptic marker NeuN
334 (NeuN/PLA$^{TrkB/SorCS2}$) for cell body localization, and PSD95 (PSD95/PLA$^{TrkB/SorCS2}$) for
335 spines localization at the stimulated areas. In TBS-slices, both NeuN/PLA$^{TrkB/SorCS2}$ and
336 PSD95/PLA$^{TrkB/SorCS2}$ colocalizations had significantly increased with respect to baseline
337 stimulation, indicating that TrkB and SorCS2 aggregate at post-synaptic sites in response
338 to potentiating conditions. The astrocytic dependency on TrkB/SorCS2 aggregation was
339 next examined in TBS-slices from p75-flox mice previously injected with control LV-
340 GFP^{stop} or LV-BDNFpro^{stop} viruses. TBS-slices transduced with LV-BDNFpro^{stop} showed
341 higher levels of NeuN/PLA$^{TrkB/SorCS2}$ signals with respect to slices transduced with LV-
342 GFP^{stop} (Fig. 7a). Thus, BDNFpro sourced by astrocytes increases TrkB/SorCS2
343 aggregation at post-synaptic sites following LTP-inducing neuronal stimulation.
344 Finally, high-localized TrkB/SorCS2 aggregation would result in increased TrkB activity.
345 To assess this possibility, we examined TrkB phosphorylation (pTrkB) by using α-
346 phospho-TrkB (Tyr816) antibody (αpTrkB). Given that pTrkB is essentially a fraction of

the total TrkB levels, we measured, in a quantitative analysis, pTrkB that colocalizes with TrkB immunoreactivity. We found that the levels of pTrkB/TrkB colocalization had significantly increased in TBS-slices compared to non-stimulated slices from p75-flox mice injected with LV-BDNFpro^{stop} or TBS-stimulated slices from control littermates injected with LV-GFP^{stop} (Fig. 7b and Supplementary Fig. 7). Moreover, this increase is comparable to the one observed in TBS vs. baseline condition in control littermates (Fig. 7b). Thus, astrocytic BDNFpro recruits TrkB expression on adjacent spines for tight temporal, spatial and stimulus- dependent TrkB phosphorylation.

Astrocytic BDNFpro restores memory retention

Substantial evidence suggests that the perirhinal cortex plays a critical role in familiarity-based object recognition (ORT) memory (43, 44).

To assess whether BDNFpro originated by astrocytes is involved in recognition memory in vivo, we injected LV-GFP^{stop} or LV-BDNFpro^{stop} viruses in perirhinal cortex of p75-flox mice the last day of tamoxifen treatment and performed the ORT 14 dptm. Mice performed the ORT with a retention interval between the sample phase and the test phase of 10 min and 24 h (Fig. 8a). The discrimination index (DI) can vary between +1 and -1, where positive scores indicate more time spent with the novel object and a zero or negative score indicates equal or less time spent with the novel object. In the DI (Fig. 8b) p75-flox mice injected with control virus showed positive values at 10 min time that decreased to almost zero at 24 h. Thus, when astrocytic proBDNF uptake was blocked, as in p75-flox mice, memory consolidation was prevented and mice showed a significant memory deficit in the ORT (15). Strikingly, p75-flox mice injected with a virus transducing BDNFpro showed similar positive value at both 10 min and 24 h times, as for control littermates, indicating that astrocytic BDNFpro is sufficient for the consolidation of this type of memory. Exploration time at the sample phase was comparable between groups (Fig. 8c). Thus, BDNFpro in astrocytes could reverse the memory defect exhibited by p75-flox mice, demonstrating its necessity to memory consolidation in vivo.

Discussion

At the micro/nanoscale, neural plasticity emerges as changes in the spatiotemporal pattern of activation of different synaptic components. While much attention has been given to pre- and post-synaptic sites for coordinating long-lasting synaptic strengthening (6, 11), research in this regard has long time ignored the function of astrocytic microdomains. The close anatomical interface between pre- and post-synaptic neurons and astrocytes has been referred to as the "synaptic triate" (45) or "tri-partite synapse" (46) in which astrocytic microdomains are proposed as regulatory units of neuron-glia interaction. Our work indicates these cellular structures to be specialized in prolonging synaptic potentiation by clearing and converting the inactive proBDNF in functional BDNFpro and mBDNF products, thereby increasing temporal, spatial and stimulus-dependent neurotrophin availability at spines. BDNFpro and mBDNF reinforce TrkB signaling *via* adaptive molecular mechanisms that promote LTP maintenance and memory consolidation. This molecular functionalization process might involve individual or small groups of synapses covered by *thin* (nanometer scale) or *thick* (~10-15 μm^2) microdomains, respectively (31, 47, 48). It is worthy of note that the dimensions of *thick* microdomains coincide with the reported maximum distance between functionally related spines (49). Studies on neurons in the visual cortex have recently reported that dendritic spines, within less than ±10 μm^2 distance, tend to share receptive field properties, while more distant spines are functionally uncorrelated (50). It is therefore reasonable to assume that the spatial extent of BDNFpro localization at microdomains might be a constraining factor for the effect of these substructures in synaptic modifications. This spatially restricted mechanism of plasticity may finally participate in long-term memory engram formation (51) and memory capacity (52).

Confinement of a molecular memory in astrocytic microdomains

Astrocytic proBDNF is inactive in the precursor state and can be converted to active mBDNF at microdomains. This inactive-to-active transition increases mBDNF availability exceeding the transient, activity-dependent neurotrophin secretion from neurons. This represents *per se* a positive cellular and molecular loop (proBDNF transfer

from neurons to astrocytes ==> processing and storage of the precursor ==> mBDNF transfer from astrocytes to neuron) that survives to LTP induction. However, our data provide further significance to this molecular activation; not only mBDNF, but also the BDNFpro turned out to possess an independent function. Once generated, this byproduct participates in astrocytic recycling by inducing changes in TrkB levels (Fig. 7a) as well as in this receptor phosphorylation at post-synaptic sites (Fig. 7b). Thus, BDNFpro operates synaptic adaptations once LTP is expressed that are relevant for its later stabilization (Fig. 5a, c). Mechanistically, BDNFpro acts as an activator of TrkB/SorCS2 aggregation by spine targeting (Fig. 6b-d). This is a new physiological role attributed to the cleaved BDNFpro, which on behalf of its structural instability has been recently assigned to co-secretion with mBDNF (37, 41) and assumed to possess independent physiological functions (24, 53). While previous data reported that exogenous application of proBDNF (12) or BDNFpro (53) enhances long-term depression (LTD)-inducing low frequency-stimulation in the hippocampus, we provide compelling evidence that in perirhinal cortex astrocytic proBDNF recycling and therefore astrocytic release of its proteolytic products BDNFpro and mBDNF do not participate in this form of facilitation (15). This emphasizes the relevance to consider different brain regions and to identify the precise location of neurotrophin secretion at synaptic level. Although extremely challenging experimentally, these important issues must be addressed in order to clarify current inconsistency of the involvement of neurotrophins in synaptic plasticity and processes related to memory (54).

Overall, the main question underlying astrocytic proBDNF processing can be further detailed: is the persistence in synaptic strength due to an additional supply of active mBDNF from astrocytic microdomains or is it due to an increase in the post-synaptic response to this neurotrophin by the prodomain? We suggest cooperation between BDNFpro and mBDNF for convergent, but independent post-synaptic signaling. On the one hand, exogenous administration of mBDNF could restore LTP deficit in p75-flox mice (15), implicitly assuming that mBDNF supplied by astrocytes is sufficient for LTP maintenance. On the other hand, astrocytic expression of the sole BDNFpro in p75-flox slices (Fig. 5a) or its exogenous administration (Fig. 5c) equally rescued the LTP deficits.

This suggests a mechanism, in which the basal levels of TrkB at spines cannot recruit sufficient mBDNF signaling for LTP maintenance. On recycling, BDNFpro increases TrkB levels at post-synaptic sites, allowing the receptor to act as a central controller. Accordingly, BDNF-TrkB signaling induces molecular adaptation underlining long-lasting synaptic strengthening (11) and shapes structural plasticity (55) *via* both TrkB tyrosine (56) and serine/threonine phosphorylation (57). While this essential regulation saturates over time, the rescuing effect on LTP deficits by BDNFpro persists for the entire duration of the early-phase LTP expression, ending up at the initiation of the late-phase potentiation (Supplementary Fig. 6c). In marked contrast, mBDNF is only required for the first 10-20 min after stimulation, which is the predicted time of astrocytic proBDNF recycling (15). Thus, prodomain and mature BDNF integrate various signaling pathways once LTP is expressed, and the conversion of the precursor acts as an inducible "molecular switch". Therefore, proteolytic cleavage of pro-neurotrophins is an important regulatory step for the direction of neurotrophin function. In conclusion, proBDNF processing does not fully accomplish the classical model of self-sustained molecular alteration (1); instead, it offers a switching mechanism from one inactive state to multi-functional one. This specifies strengthening mechanism for a persistent post-synaptic signaling, as it is required for a "molecular memory" to maintain LTP.

Spine targeting of TrkB tackles the underlying changes that occur at the synapse once LTP is expressed, reinforcing the common knowledge that LTP maintenance take place post- synaptically (6). However, our data also provide evidence that the molecular basis responsible for these changes can be confined elsewhere. To understand the molecular foundation of LTP maintenance, it is therefore essential to know from which site of the synapse the "molecular memory" is originated. Since the discovery of LTP, most studies focused on whether pre- and/or post-synaptic sites are the compartments confining molecular modifications relevant for LTP maintenance; here we moved away from neurons and demonstrated that astrocytic microdomains are a central player for memory storage. Focus on the site of expression of BDNFpro was made possible by using electron microscopy (Fig. 3). BDNFpro-gold particles were seen at pre- and post-synaptic terminals and astrocytic microdomains closely interacting with these synaptic complexes.

Gold particles residing in these synaptic sites account for highly intricate trafficking events induced by TBS: BDNFpro could be (i) synthesized at pre- and/or post-synaptic sites; (ii) transported to pre- and/or post-synaptic sites; (iii) internalized in pre- and/or post-synaptic compartments as well as in astrocytic microdomains. Given this complexity, it is of note that BDNFpro localization at astrocytic microdomains is the only relevant localization required for LTP maintenance. Although EM analysis showed a variety of synapses in terms of shapes and sizes, the one thing that was constant was the enrichment of BDNFpro-gold particle at peri-synaptic astrocytes (Fig. 3). This suggests the general occurrence of proteolytic conversion in this specialized area. Moreover, BDNFpro colocalized with the SNARE protein Vamp2 (Fig. 4 a, b) and intoxication with TeTN - a protease known to cleave Vamp2 - inhibited BDNFpro secretion (Fig. 5b). This indicates that astrocytic vesicles store the processed neurotrophins at a place that is functional to synaptic use. Thus, astrocytic vesicles could serve as a reservoir of functional neurotrophin products that are available for synaptic needs. Such a modified and stable enrichment of astrocytic microdomains could serve as signaling hub of potentiated synapses providing an appealing model for information storage.

Astrocytic microdomains regulate BDNF specificity

The observation that persistent LTP and its associated synaptic changes are synapse-specific (58) raises the issue of how BDNF availability can be independently regulated in individual synapses. If BDNF could leak from a stimulated synapse, it would then massively, but incorrectly activate many additional synapses in spite of an appropriate stimulation. The idea of “synaptic capture” appears to be a valuable model in this context (58, 59). This implies that newly synthesized BDNF by neurons is delivered to all synapses, but it is only used at synapses that have been tagged by activity. In accord to this model, TrkB, the correlated molecular tag for mBDNF (60), could capture mBDNF at selected synapses. Our finding that astrocytic BDNFpro increases TrkB/SorCS2 aggregation at the spine surface (Fig. 6b and Fig. 7a), supports the idea that proBDNF processing in microdomains may cooperate to selectively tag activated synapses. This specific process will then provide the capture of mBDNF for enhancing TrkB

phosphorylation (Fig. 7b). Direct demonstration of the astrocytic origin of TrkB tagging would need to perform a two-pathway experiment (60) in perirhinal cortex of p75-flox mice; a brain area not permissive for this type of recording. However, this experiment conducted in hippocampus (42) confirmed that SorCS2 binds TrkB to facilitate TrkB/SorCS2 translocation at posts-synaptic sites for both synaptic tagging and LTP maintenance. Overall, our data suggest that astrocytic BDNFpro triggers mBDNF capture via TrkB tagging; thereby increasing selectivity and responsiveness to the neurotrophin at potentiated synapses.

Linking LTP maintenance to memory consolidation

The proposed critical role and mode of action of astrocytic proBDNF processing for LTP maintenance can be extended to long-lasting memory. Specifically, is proBDNF conversion important for memory consolidation? And as a consequence of this, is BDNFpro central to this type of memory? We demonstrated that viral expression of BDNFpro in perirhinal cortex of p75- flox mice resulted in mice that spent more time exploring a novel object than a familiar one during the 24 h-test phase (Fig. 8b). Astrocytic release of this "byproduct" is then correlated to long-lasting memory of the task. This finding supports the idea that astrocytic microdomains participate to changes in the strength of neuronal connections contributing to the most attractive cellular model for learning and memory, first defined by Hebb in 1949 (61). His hypothesis that synaptic strengthening for learning and memory occurs as a consequence of coincident activity between pre- and post-synaptic compartment now requires the integration of a new player, the astrocytic microdomains. This cyto-architectural structure accounts on functionally isolated subcellular domains that facilitate local homeostasis by redistributing ions, removing neurotransmitters, and releasing factors to influence moment-to-moment synaptic activity (8, 62). Our identification of an astrocytic "molecular memory" indicates that microdomains are also capable of sensing and integrating signals for persistent synaptic strengthening that are involved in memory consolidation in the brain. There is now overall agreement that persistent modification of the synaptic strength, *via* sustained LTP, represents a primary mechanism for the

formation of memory engrams (63). The contribution of astrocytes to synaptic engrams has been largely ignored in the past (9, 64, 65); however, it is evident that astrocytes appear to be an important cellular interface to control and modify neuronal data processing by their close physical contact with synapses (66). Astrocytic microdomains could then provide local support over synaptic potentiation and the global control of neuronal ensembles engaged in memory circuits. Thus, cortical astrocytes possess unique features that ideally position them for locally responding to synaptic demand and to sense the surrounding neuronal network activity. In this way, they can operate integrative functions for learning and memory.

Methods

Experimental models

All experiments were performed in accordance with European Union guidelines as approved by the institutional animal care and utilization committee (authorizations n°507/2017-PR; 76/2020 PR). p75-flox mice were generated by crossing loxP-p75^{NTR}-loxP mice kindly provided by B. (University of Michigan School of Dentistry, USA) with GLAST-CreER^{T2} Rosa-CAGloxP-stop-loxP(LSL)-R26R mice kindly provided by Prof. M Gotz (LMU, Munich, Germany). GFAP-GFP mice were kindly provided by Prof. A. Buffo (NICO, Torino, Italy). Animals were housed in a 12 h light/dark cycle with unrestricted access to food and water. For timed pregnancies, the plug date was designated as E0 and the date of birth was defined as P0.

Tamoxifen treatment

Male mice from p75-flox and control littermates were treated with 1 mg of tamoxifen (Sigma Aldrich, Cat#T5648) dissolved in corn oil twice a day for 5 consecutive days at age between P35 and P50.

Stereotaxic surgery

For virus delivery, 0 or 12 days after the last day of tamoxifen administration, mice were deeply anesthetized and viral particle (1 µl in volume) was infused into perirhinal cortex from each hemisphere (coordinates from Bregma: anteroposterior - 2 mm, lateral ± 4,2 mm, ventral + 2,8 mm). Viral delivery was obtained through the insertion of capillary glasses (WPI) connected to a manual syringe pump (Narishige). Mice were allowed to recover and housed in standard cages until the day of sacrifice.

Viral vectors

pAAV.GFA104.PI.eGFP.WPRE.bGH (AAV-GFAP-GFP) adenoviral vector was used to express GFP in astrocytes specifically. This vector was a gift from Philip Haydon (Addgene viral prep # 100896-AAV5; http://n2t.net/addgene:100896; RRID: Addgene_100896).

Lentiviral vectors were used for Cre-dependent expression of BDNFpro (LV-BDNFpro^{stop}), proBDNF (LV-proBDNF^{stop}), proBDNF^{CR} (LV-proBDNF^{CRstop}) and light-chain of Tetanus toxin (TeTN) (LV-TeTN^{stop}). Lentiviral vectors were produced starting from pLV which drives gene expression under the cytomegalovirus (CMV) promoter. A gene-cassette including GFP encoding sequence was flanked by two modified loxP sites (lox2272). This prevented the formation of unwanted ATG start codons after Cre-mediated recombination. The GFP expression was stopped by two stop codons. Next, a single EcoRV-blunt cloning site, an IRES2 (internal ribosomal entry site2) followed by TandemTomato (Tomato) was cloned in 5' direction before the WPRE lentiviral vector element. This construct showed strong GFP expression and weak expression of IRES2-Tomato. Under Cre-mediated recombination, the GFP was lost and the IRES2-Tomato cassette was under control of the promoter. Next, the EcoRV-blunt site was used to introduce the coding sequence of BDNFpro, proBDNF, proBDNF^{CR} and light-chain of Tetanus toxin (TeTN). Lentiviral particles were produced in HEK293T cells. Lentiviral expression vectors were co- transfected with the pseudotyping vector pMD2.G and the packaging vector pCMVR8.91. Lentiviral particles were separated from the supernatant by ultracentrifugation and stored at -80°C in 50 mM Tris-HCl, pH 7.4, 130 mM NaCl, 10 mM KCl, 5 mM $MgCl_2$.

Electrophysiological recording

Slices from perirhinal cortex were prepared from p75-flox, control littermates or GFAP-GFP mice. The brain was removed and placed in cold oxygenated (95% O_2 and 5% CO_2) artificial cerebrospinal fluid (ACSF) containing 124.0 mM NaCl, 4.4 mM KCl, 1 mM NaH_2PO_4, 2.5 mM $CaCl_2$, 1.3 mM $MgCl_2$, 26.2 mM $NaHCO_3$, 10 mM glucose, and 2 mM L-ascorbic acid. Horizontal cortex slices (300 μm thick) were prepared using a vibratome and maintained in a chamber containing oxygenated ACSF at room temperature. After a minimum recovery period of 1 h, a single slice was transferred into a submersion recording chamber perfused (3 ml/min) with oxygenated ACSF at 32°C ± 0.2°C; square current pulses (duration 0.2 ms) were applied every 30 s (0.033 Hz) using a stimulus generator (WPI, stimulus isolator A360) connected through a stimulus isolation

unit to a concentric bipolar electrode (40–80 KU, FHC) positioned in layers II/III on the temporal side of the rhinal sulcus. Evoked extracellular fEPSPs were recorded using an Axoclamp-2B amplifier (Axon Instruments) with ACSF-filled glass micropipette pulled on a vertical puller (Narishige PC-10, resistance [<5 MU]), inserted in layers II/III at around 500 mm from the stimulation electrode, and analyzed using Axoscope 8.0 software. Baseline responses were obtained every 30 s with a stimulus intensity adjusted to induce 50% of the maximal synaptic response. After 20 min of stable baseline, LTP was evoked by TBS (100 Hz; four sets of stimulations delivered 15 s apart, each one consisting of ten bursts of five pulses at 100 Hz with inter-burst intervals of 150 ms). fEPSPs were plotted as amplitude. Each point represents the responses every 30 s expressed as means ± SEM.

Input/output curves were produced delivering stimuli (0.1 ms duration) to the stimulation electrode with stimulation intensities from 50 to 400 μA in steps of 50 μA.

Paired-pulse facilitation was expressed as the mean ratio of second and first fEPSP amplitude as a percentage with an interstimulus interval of 25, 50, 100, 150 and 200 ms.

In some experiments, recombinant BDNFpro (10 ng/ml; Alomone Labs, Cat#B-245), $BDNFpro^{Val/Met}$ (10 ng/ml; Alomone Labs, Cat#B-445), mBDNF (10 ng/ml; Laboratory of Antonino Cattaneo, SNS, Pisa, Italy), $proBDNF^{CR}$ (20 ng/ml; Laboratory of Antonino Cattaneo, SNS, Pisa, Italy) were perfused into a recording chamber.

Immunohistochemistry

Brain slices were fixed in 4% PFA for 1 h after recording. Slices were treated with 1% Triton X-100 for 20 min, blocked with 3% BSA in PBS for 1 h and incubated overnight free-floating with primary antibodies diluted in blocking buffer. Slices were washed in PBS and incubated for 2 h at room temperature with secondary antibodies diluted in blocking buffer. Slices were eventually counterstained with DAPI (Sigma Aldrich, Cat#D9542) and mounted with Aqua Poly/mount (Polysciences, Inc., Cat #18606).

Antibodies

The following antibodies were used: rabbit α-GFP (Thermo Fisher Scientific Cat#A-6455; RRID:AB#2536208; IHC 1:1000 ICC 1:1000), chicken α-GFP (Thermo Fisher Scientific Cat#A10262; RRID:AB#2534023, IHC 1:1000), chicken α-BDNF (Promega Cat#G1641; RRID:AB#430850, IHC 1:300), rabbit α-BDNF (Alomone Labs Cat# ANT-010; RRID:AB_2039756, EM 1:20), chicken α-proBDNF (Millipore Cat#AB9042; RID:AB#2274709, IHC 1:300), rabbit α-proBDNF (Alomone Labs Cat#ANT-006; RRID:AB_2039758, EM 1:20), rabbit α-BDNFpro (Laboratory of Bai Lu, Govern Institute for Brain Research, Tsinghua University, Beijing, IHC 1:300, EM 1:20, WB 1:500), mouse α-NeuN (Abcam Cat#ab77315; RRID:AB#1566475, IHC 1:1000), guinea pig α-NeuN (Millipore Cat#ABN90; RRID:AB#11205592, IHC 1:1000), rabbit α-pTrkB (Tyr 816) (Laboratory of Moses Chao, Skirball Intitute of Biomolecular Medicine, New York, USA, IHC 1,25 mg/ml), goat α-TrkB (Santa Cruz Biotechnology Cat#sc-12-G; RRID:AB#632558, IHC 1:300), mouse α-PSD95 (Merck-Millipore Cat#MAB1596; RRID:AB_2092365, IHC 1:500), sheep α-SorCS2 (R&D system Cat#AF4238; RRID:AB_10645642), rabbit α -SorCS2 (MyBioSource Cat# MBS5302436), rabbit α-$p75^{NTR}$ (Promega Cat#G3231; RRID:AB_430853, IHC 1:1000), chicken α-GFAP (Abcam Cat#ab134436; RRID:AB_2818977, IHC 1:1000), mouse α-GFAP (Abcam Cat#ab10062; RRID:AB_296804, IHC 1:1000), mouse α-synaptobrevin2\VAMP2 (Synaptic System Cat#104 211; RRID:AB_2619758, IHC 1:300), rabbit α-beta galactosidase (Proteintech Cat#15518-1-AP; RRID:AB_2263448, IHC 1:500), rabbit α -RFP (Rockland Antibodies Cat#600-401-379; RRID:AB_2209751 IHC 1:1000), mouse α DsRed (Santa Cruz Biotechnology Cat# sc-390909; RRID:AB_2801575 IHC 1:1000).

Western blot experiments

Recombinant mBDNF, $proBDNF^{CR}$ and BDNFpro were suspended in protein sample buffer, boiled for 7 min at 95°C, resolved by 12% SDS-PAGE and transferred to nitrocellulose membranes. Membranes were incubated (1 h) at room temperature in blocking solution (5% BSA in TBS-Tween 0.1%) and incubated overnight at 4°C with primary antibodies. Membranes were washed 3 times in TBS-Tween and incubated for

1.5 h at room temperature with horseradish peroxidase (HRP)-conjugated secondary antibodies. ECL was used for detection.

Primary cell cultures

Cortices were isolated from E17.5 mouse embryos and incubated for 20 min at 37°C in Trypsin/EDTA 0.25% (Thermo Fisher Scientific, Cat#25200056). Cortical cells were dissociated with a plastic pipette, collected by centrifugation (800 RPM, 5 min) and resuspended in Dulbecco's modified Eagle's medium (DMEM; GIBCO Cat#10938025) supplemented with 10% of fetal bovine serum and Penicillin/Streptomycin (GIBCO; Cat#15070063). Cells were transfected using Amaxa Nucleofector system following manufacturer instructions and plated on glass coverslips precoated with poly-L-lysine (0.1 mg/ml; Sigma Aldrich, Cat#P6282). Three hours after plating, the medium was changed to Neurobasal (GIBCO, Cat#21103049) supplemented with B27-supplement (GIBCO, Cat#17504044) and Penicillin/Streptomycin/Glutamine (GIBCO, Cat#1038016).

Proximity ligation assay (PLA)

PLA was performed on fixed mouse primary cortical neurons non-permeabilized and on fixed perirhinal sections permeabilized with Triton X 1 % for 20 minutes. PLA was performed following manufacturer instruction (Duolink PLA Sigma Aldrich). Briefly samples were blocked with 3% BSA in PBS for 1 hour and incubated with primary antibodies at 4°C overnight. Samples were washed with PBS and incubated with PLA probes MINUS (Duolink PLA Probe Anti-Goat MINUS antibody, Sigma Aldrich Cat# DUO92006) and PLUS (Duolink PLA Probe Anti-Rabbit PLUS antibody, Sigma Aldrich Cat# DUO92002) for 1 h at 37°C. The PLA probes were diluted (1:5) in antibody diluent. Samples were washed in 1X buffer A 2X5 min under gentle agitation and incubated with ligation- ligase solution for 30 min at 37°C. Samples were washed in 1X wash buffer for 2X2 min under gentle agitation and incubated with amplification polymerase solution for 90 min at 37°C. In some experiments, we performed immunodetection over PLA incubating PLA samples with secondary antibodies coupled with the appropriate

fluorophores for 2 h at room temperature. Samples were washed in 1X wash buffer B for 2X 10 min and with 0.01 X wash buffer B for 1 min. Samples were mounted with Prolong Gold antifade reagent with DAPI.

Confocal microscopy and quantitative image analysis

Confocal imaging was performed using a laser-scanning motorized confocal system (Nikon A1) equipped with an Eclipse Ti-E inverted microscope and four laser lines (405, 488, 561 and 638 nm). Z-series images were taken with an inter-stack interval of 0.5 µm using 60X oil objective. For each type of quantification, laser intensities and camera settings were maintained identically within the same experiment to allow the comparison of different experimental groups and treatments. Image processing and 3D-rendering were performed using the software NIS Element (Nikon). Colocalizations (BDNFpro/GFP; Vamp2-GFP; BDNFpro/Vamp2; TrkB/pTrkB; $PLA^{TrkB/SorCS2}$/NeuN; $PLA^{TrkB/SorCS2}$/PSD95) were quantified calculating Mander's overlap or Pearson's correlation using the software NIS Element (Nikon). Colocalization data for the comparison of stimulated slices (TBS) vs. non-stimulated slices (baseline) are expressed following normalization of the Mander's overlap of each treatment to the average of Mander's overlap of the baseline.

3D-SIM

3D-SIM was performed using X-Light V2 confocal spinning disk system completed with a Video Confocal super-resolution module (CrestOptics, Italy) with a lateral resolution of 115 nm and an axial resolution of ~250 nm. The system was equipped with a 60x/1.40 NA PlanApo Lambda oil immersion objective (Nikon, Japan), Zyla sCMOS camera (Andor) and Spectra X Lumencor LEDs Light Source with bandpass excitation filters of 460-490 and 535-600 nm (Chroma Technology, US). Image stacks were acquired with a format of 2048x2048 pixels and a z-distance of 150 nm and with 36 raw SIM images per plane (multiple acquisition mode x-y grid scan). The SIM raw data with 16-bit depth were computationally reconstructed using the Metamorph software package. For 3D-image rendering and colocalization analysis, images were processed using NIS-Elements

software. Quantification of BDNFpro/GFP puncta was performed manually counting the number of immunoreactive puncta in finger-like extension and lamellar sheaths compared to the total number of puncta found in astrocytes (for these experiments n=6 cells, 3 slices, 3 mice for each condition).

Electron microscopy

Sections (300 µm) from electrophysiological recordings were fixed in a solution of 4% PFA and 0.1 % glutaraldehyde in 0.1 M phosphate buffer (PB) for 4 hours and then washed overnight in 50 mM TBS, pH 7.4. Slices were immersed for 2 h in a cryoprotecting solution (25% sucrose and 10% glycerol in 0.05 M PB) before being snap frozen in liquid nitrogen-cooled isopentane. After washing in 0.1 M PB, sections were incubated for 1 h in 20% normal goat serum in TBS. Slices were then incubated for three nights at 4°C in a 3% BSA/TBS solution containing primary αBDNFpro or αmBDNF or αproBDNF. Sections were incubated overnight at 4°C in 3% BSA/TBS solution containing 2 nm-gold conjugated goat arabbit (BBI International). Sections were rinsed in TBS and then fixed for 30 min in a 2,5% glutaraldehyde solution and post-fixed with 1% osmium tetroxide. After dehydration in an ethanol series followed by propylene oxide, samples were embedded in Epon812 epoxy resin and observed with a JEOLJEM-1011 transmission electron microscope, operated at 100 kV, after cutting ultrathin sections (60 nm thick). Negative controls were performed in the absence of primary antibody.

Astrocytes were identified using 3 structural criteria: (i) localization between synapses: the space between synapses is occupied by astrocytic processes. Astrocytes are indeed cellular structures just filling all the space between synapses, dendrites, and axons; (ii) irregular, stellate shape: the processes of astrocytes surrounding synaptic contacts often adopt quite convoluted forms. In comparison to their flatter neuronal counterparts, perisynaptic astrocytes show an irregular profile; (iii) relatively clear cytoplasm: the cytoplasm of an astrocyte differs from that of neighboring objects in the neuropil. An astrocyte cytoplasm is less electron-dense than the one of neurons. Quantification of gold grains was performed manually counting the number of gold grains in a membrane

delimited area of 230 nm radius surrounding synaptic contacts compared to the total number of gold grains found in astrocytes (for these experiments n= 5 slices; 3 mice).

Object recognition test (ORT)

ORT was performed in a Y-apparatus with high, homogenous white walls, 30 cm high: one arm was used as start arm and had a sliding door to control access to the arena; the other two arms were used to display the objects. The start arm is 26 cm in length with the sliding door placed at 13 cm, and the lateral arms are 18 cm long. All arms are 10 cm wide. On the first day (habituation day) mice explored the arena for 20 min. The following day, the learning session (sample phase) was performed: for five minutes the animals were free to explore the arena, which contained two identical objects, one for each arm, placed at the end of the arm. At 10 min or 24 h after the sample phase, the test phase was run; the animals were free to explore the arena containing two objects, the familiar object and a novel one. Arena and objects were cleaned up between trials to stop the build-up of olfactory cues. The discrimination index was calculated as follows: (TNew - TOld)/(TNew + TOld), with TNew and TOld being the time spent exploring the new and the familiar objects, respectively. A video camera was mounted above the apparatus to record trials with the EthoVision software (Noldus). The exploration time was taken as the time during which mice approached the objects with muzzle and paws.

Statistics and reproducibility

All data were run for a normality test before a statistical comparison test. Data normally distributed were summarized by mean ± SEM. Comparison between two different groups was assessed by an unpaired t-test. For ORT discrimination index, two-way ANOVA followed by a Holm-Sidak method test was used. The level of significance used was $p < 0.05$.

Data availability

The authors declare that all data supporting the findings of this study are available within the paper and its supplementary information files.

References

1. F. Crick, Neurobiology: Memory and molecular turnover. *Nature* **312**, 101–101 (1984).
2. J. E. Lisman, M. A. Goldring, Feasibility of long-term storage of graded information by the Ca2+/calmodulin-dependent protein kinase molecules of the postsynaptic density. *Proc. Natl. Acad. Sci.* **85**, 5320–5324 (1988).
3. K. Kim, T. Saneyoshi, T. Hosokawa, K. Okamoto, Y. Hayashi, Interplay of enzymatic and structural functions of CaMKII in long-term potentiation. *J. Neurochem.* **139**, 959–972 (2016).
4. S. Miller, Regulation of brain Type II Ca2+/calmodulin-dependent protein kinase by autophosphorylation: A Ca2+-triggered molecular switch. *Cell* **44**, 861–870 (1986).
5. K. Si, E. R. Kandel, The Role of Functional Prion-Like Proteins in the Persistence of Memory. *Cold Spring Harb. Perspect. Biol.* **8**, a021774 (2016).
6. R. A. Nicoll, A Brief History of Long-Term Potentiation. *Neuron* **93**, 281–290 (2017).
7. N. J. Allen, Astrocyte regulation of synaptic behavior. *Annu. Rev. Cell Dev. Biol.* **30**, 439–63 (2014).
8. A. Araque, *et al.*, Gliotransmitters travel in time and space. *Neuron* **81**, 728–739 (2014).
9. R. D. Fields, *et al.*, Glial Biology in Learning and Cognition. *Neurosci.* **20**, 426–431 (2014).
10. V. Lessmann, T. Brigadski, Mechanisms, locations, and kinetics of synaptic BDNF secretion: an update. *Neurosci. Res.* **65**, 11–22 (2009).
11. H. Park, M. Poo, Neurotrophin regulation of neural circuit development and function. *Nat. Rev. Neurosci.* **14**, 7–23 (2013).
12. B. Lu, P. T. Pang, N. H. Woo, The yin and yang of neurotrophin action. *Nat. Rev. Neurosci.***6**, 603–14 (2005).
13. M. Bergami, *et al.*, Uptake and recycling of pro-BDNF for transmitter-induced secretion by cortical astrocytes. *J. Cell Biol.* **183**, 213–221 (2008).
14. S. Manju, B. Vignoli, M. Canossa, R. Blum, Neurobiology of local and intercellular BDNF signaling. *Pflugers Arch. Eur. J. Physiol.* (2017).
15. B. Vignoli, *et al.*, Peri-Synaptic Glia Recycles Brain-Derived Neurotrophic Factor for LTP Stabilization and Memory Retention. *Neuron* **92** (2016).
16. D. Lanjakornsiripan, *et al.*, Layer-specific morphological and molecular differences in neocortical astrocytes and their dependence on neuronal layers. *Nat. Commun.* **9**, 1623 (2018).
17. B. Vignoli, M. Canossa, Glioactive ATP controls BDNF recycling in cortical astrocytes. *Commun. Integr. Biol.* **10** (2017).
18. J. Boutilier, *et al.*, Proneurotrophins require endocytosis and intracellular

proteolysis to induce TrkA activation. *J. Biol. Chem.* **283**, 12709–16 (2008).

19. H. Rösch, R. Schweigreiter, T. Bonhoeffer, Y.-A. Barde, M. Korte, The neurotrophin receptor p75NTR modulates long-term depression and regulates the expression of AMPA receptor subunits in the hippocampus. *Proc. Natl. Acad. Sci. U. S. A.* **102**, 7362–7 (2005).

20. N. H. Woo, *et al.*, Activation of p75NTR by proBDNF facilitates hippocampal long-term depression. *Nat. Neurosci.* **8**, 1069–77 (2005).

21. P. I. Ortinski, *et al.*, Selective induction of astrocytic gliosis generates deficits in neuronal inhibition. *Nat. Neurosci.* **13**, 584–591 (2010).

22. L. Zhuo, *et al.*, Live Astrocytes Visualized by Green Fluorescent Protein in Transgenic Mice. *Dev. Biol.* **187**, 36–42 (1997).

23. G. Aicardi, *et al.*, Induction of long-term potentiation and depression is reflected by corresponding changes in secretion of endogenous brain-derived neurotrophic factor. *Proc. Natl. Acad. Sci. U. S. A.* **101**, 15788–92 (2004).

24. P. T. Pang, G. Nagappan, W. Guo, B. Lu, Extracellular and intracellular cleavages of proBDNF required at two distinct stages of late-phase LTP. *npj Sci. Learn.* **1**, 16003 (2016).

25. J. S. Aaron, A. B. Taylor, T.-L. Chew, Image co-localization – co-occurrence versus correlation. *J. Cell Sci.* **131**, jcs211847 (2018).

26. V. Lessmann, K. Gottmann, M. Malcangio, Neurotrophin secretion: current facts and future prospects. *Prog. Neurobiol.* **69**, 341–374 (2003).

27. E. Bogenmann, *et al.*, Generation of mice with a conditional allele for the p75(NTR) neurotrophin receptor gene. *Genesis* **49**, 862–869 (2011).

28. T. Mori, *et al.*, Inducible gene deletion in astroglia and radial glia--a valuable tool for functional and lineage analysis. *Glia* **54**, 21–34 (2006).

29. P. Soriano, Generalized lacZ expression with the ROSA26 Cre reporter strain. *Nat. Genet.* **21**, 70–71 (1999).

30. E. Zuccaro, *et al.*, Polarized expression of p75(NTR) specifies axons during development and adult neurogenesis. *Cell Rep.* **7**, 138–52 (2014).

31. J. Grosche, *et al.*, Microdomains for neuron–glia interaction: parallel fiber signaling to Bergmann glial cells. *Nat. Neurosci.* **2**, 139–143 (1999).

32. B. Fernandez, I. Suarez, G. Gonzalez, Topographical distribution of the astrocytic lamellae in the hypothalamus. *Anat. Anz.* **156**, 31–7 (1984).

33. B. S. Khakh, M. V Sofroniew, Diversity of astrocyte functions and phenotypes in neural circuits. *Nat. Neurosci.* **18**, 942–952 (2015).

34. I. Patrushev, N. Gavrilov, V. Turlapov, A. Semyanov, Subcellular location of astrocytic calcium stores favors extrasynaptic neuron–astrocyte communication. *Cell Calcium* **54**, 343–349 (2013).

35. N. Gavrilov, *et al.*, Astrocytic Coverage of Dendritic Spines, Dendritic Shafts, and Axonal Boutons in Hippocampal Neuropil. *Front. Cell. Neurosci.* **12** (2018).

36. V. Montana, E. B. Malarkey, C. Verderio, M. Matteoli, V. Parpura, Vesicular

transmitter release from astrocytes. *Glia* **54**, 700–715 (2006).

37. S. Dieni, *et al.*, BDNF and its pro-peptide are stored in presynaptic dense core vesicles in brain neurons. *J. Cell Biol.* **196**, 775–88 (2012).

38. M. F. Egan, *et al.*, The BDNF val66met Polymorphism Affects Activity-Dependent Secretion of BDNF and Human Memory and Hippocampal Function. *Cell* **112**, 257–269 (2003).

39. S.-J. Tsai, Critical Issues in BDNF Val66Met Genetic Studies of Neuropsychiatric Disorders. *Front. Mol. Neurosci.* **11** (2018).

40. Z.-Y. Chen, Variant Brain-Derived Neurotrophic Factor (BDNF) (Met66) Alters the Intracellular Trafficking and Activity-Dependent Secretion of Wild-Type BDNF in Neurosecretory Cells and Cortical Neurons. *J. Neurosci.* **24**, 4401–4411 (2004).

41. A. Anastasia, *et al.*, Val66Met polymorphism of BDNF alters prodomain structure to induce neuronal growth cone retraction. *Nat. Commun.* **4**, 2490 (2013).

42. S. Glerup, *et al.*, SorCS2 is required for BDNF-dependent plasticity in the hippocampus. *Mol. Psychiatry* **21**, 1740–1751 (2016).

43. M. W. Brown, J. P. Aggleton, Recognition memory: what are the roles of the perirhinal cortex and hippocampus? *Nat. Rev. Neurosci.* **2**, 51–61 (2001).

44. E. A. Murray, T. J. Bussey, L. M. Saksida, Visual perception and memory: a new view of medial temporal lobe function in primates and rodents. *Annu. Rev. Neurosci.* **30**, 99–122 (2007).

45. T. J. Kettenmann H, Faissner A, "Comprehensive Human Physiology" in R. Greger, U. Windhorst, Eds. (Springer Berlin Heidelberg, 1996).

46. A. Araque, R. P. Sanzgiri, V. Parpura, P. G. Haydon, Astrocyte-induced modulation of synaptic transmission. *Can. J. Physiol. Pharmacol.* **77**, 699–706 (1999).

47. M. A. Di Castro, *et al.*, Local Ca2+ detection and modulation of synaptic release by astrocytes. *Nat. Neurosci.* **14**, 1276–1284 (2011).

48. J. Grosche, H. Kettenmann, A. Reichenbach, Bergmann glial cells form distinct morphological structures to interact with cerebellar neurons. *J. Neurosci. Res.* **68**, 138–149 (2002).

49. I. Polykretis, V. Ivanov, K. P. Michmizos, "The Astrocytic Microdomain as a Generative Mechanism for Local Plasticity" in In: Wang S. et al., Eds. (Brain Informatics. BI, Lecture Notes in Computer Science, vol 11309. Springer, Cham., 2018).

50. B. Scholl, D. E. Wilson, D. Fitzpatrick, Local Order within Global Disorder: Synaptic Architecture of Visual Space. *Neuron* **96**, 1127-1138.e4 (2017).

51. A. Govindarajan, R. J. Kelleher, S. Tonegawa, A clustered plasticity model of long-term memory engrams. *Nat. Rev. Neurosci.* **7**, 575–83 (2006).

52. P. Poirazi, B. W. Mel, Impact of Active Dendrites and Structural Plasticity on the Memory Capacity of Neural Tissue. *Neuron* **29**, 779–796 (2001).

53. T. Mizui, *et al.*, BDNF pro-peptide actions facilitate hippocampal LTD and are altered by the common BDNF polymorphism Val66Met. *Proc. Natl. Acad. Sci.* **112**, E3067–E3074 (2015).

54. M. Song, K. Martinowich, F. S. Lee, BDNF at the synapse: why location matters. *Mol. Psychiatry* **22**, 1370–1375 (2017).

55. A. K. Fu, N. Y. Ip, Regulation of postsynaptic signaling in structural synaptic plasticity. *Curr. Opin. Neurobiol.* **45**, 148–155 (2017).

56. L. Minichiello, *et al.*, Mechanism of TrkB-mediated hippocampal long-term potentiation. *Neuron* **36**, 121–37 (2002).

57. K.-O. Lai, *et al.*, TrkB phosphorylation by Cdk5 is required for activity-dependent structural plasticity and spatial memory. *Nat. Neurosci.* **12** (2012).

58. U. Frey, R. G. Morris, Synaptic tagging and long-term potentiation. *Nature* **385**, 533–6 (1997).

59. R. G. M. Morris, Elements of a neurobiological theory of hippocampal function: the role of synaptic plasticity, synaptic tagging and schemas. *Eur. J. Neurosci.* **23**, 2829–2846 (2006).

60. Y. Lu, *et al.*, TrkB as a Potential Synaptic and Behavioral Tag. *J. Neurosci.* **31**, 11762–11771 (2011).

61. D. O. Hebb, *The organization of behavior; a neuropsychological theory* (Wiley, 1949).

62. E. Blanco-Suárez, A. L. M. Caldwell, N. J. Allen, Role of astrocyte–synapse interactions in CNS disorders. *J. Physiol.* **595**, 1903–1916 (2017).

63. M. Poo, *et al.*, What is memory? The present state of the engram. *BMC Biol.* **14**, 40 (2016).

64. A. Adamsky, I. Goshen, Astrocytes in Memory Function: Pioneering Findings and Future Directions. *Neuroscience* **370**, 14–26 (2018).

65. P. J. Gebicke-Haerter, Engram formation in psychiatric disorders. *Front. Neurosci.* **8** (2014).

66. L. E. Clarke, B. A. Barres, Emerging roles of astrocytes in neural circuit development. *Nat. Rev. Neurosci.* **14**, 311–321 (2013).

Acknowledgments

We thank Massimo Gamberini and Silvia Biggi for technical assistance and Ranzi Barbara for lab management; Moses Chao for providing pTrkB antibody; Brian A. Pierchala for providing $p75^{lox/lox}$ mice; Antonino Cattaneo for providing recombinant BDNF and $proBDNF^{CR}$; Magdalena Götz for providing GLAST-$CreER^{T2}$ mice; Annalisa Buffo for providing GFAP-GFP mice; IN-BDNF consortium for scientific support.

This project received founding from Progetti di Ricerca di Rilevanza Nazionale (PRIN), Bando 2017 Project number 2017HPTFFCPRIN to M.C.; European Research Council (ERC) under the European Union's Horizon 2020 research and innovation program (grant agreement N° 788793-BACKUP) to M.C. and B.V.; Deutsche Forschungsgemeinschaft BL567/3- 2 and project number 44541416–TRR58–A10 to R.B.; Graduate School of Life Sciences (GSLS) Würzburg fellowship to M.S.; Fondazione Umberto Veronesi post-doctoral grant 2018 to B.V.

Author contributions

Conceptualization: B.V. and M.C.; Investigation; B.V., S.S., M.S., and G.S.; Writing-original draft: B.V. and M.C.; Writing-review and editing; R.B. and B.L.; Supervision: R.B., S.S. and N.B.; Funding acquisition: M.C., B.V. and R.B.; Resources: B.L., R.B and S.S.

Competing interest

The authors declare no competing interests.

Figures

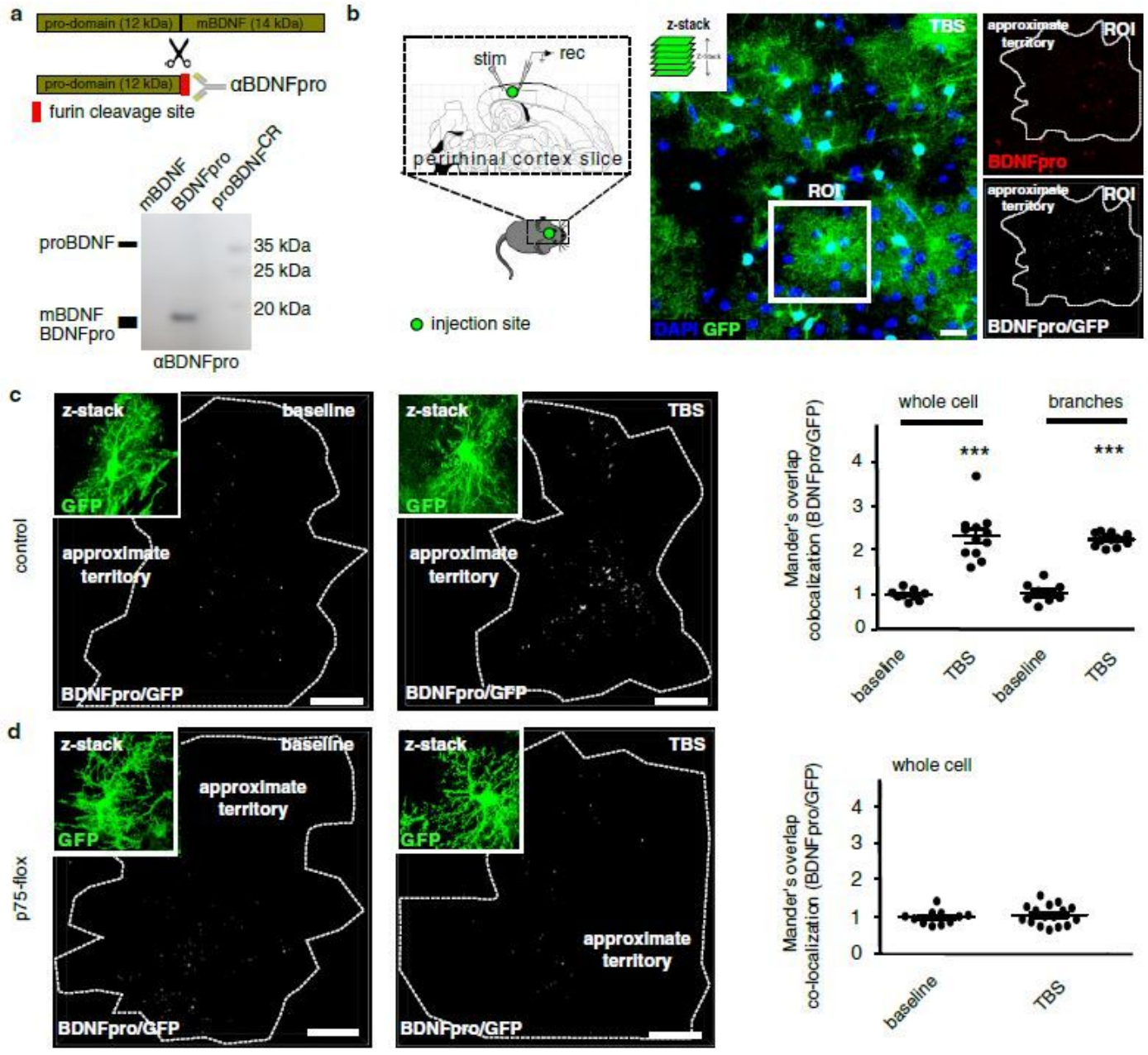

Figure 1

proBDNF processing in cortical astrocytes (a) Schematic representation of proBDNF precursor and cleaved BDNFpro domain (upper). αBDNFpro antibody recognizes the furin cleavage site of the prodomain. Western blotting probing recombinant mBDNF, BDNFpro and proBDNFCR with αBDNFpro antibody (lower). (b) Cortical slices from control mice injected with AAV-GFAP-GFP virus were recorded and fixed 10 min after TBS for immunostaining (left). z-stack reconstruction shows astrocytes labeled by GFP (middle). Three times magnification of a single stack from a region of interest (ROI) (right) show

BDNFpro immunoreactivity (upper) and BDNFpro/GFP colocalization signal (lower) of one GFP-astrocyte delimited by an approximate territory (white dashed). Scale bar: 10 µm. (c) z-stack reconstruction of BDNFpro/GFP colocalization signals in astrocytes from baseline- and TBS-slices from control mice. The insets show GFP signal. BDNFpro/GFP colocalization was quantified in the whole cell and branches using Mander's overlap. Data are normalized to baseline and presented as mean ± SEM. *** p<0.001 (Unpaired t-test); (n = 9 cells, 4 slices, 3 mice for baseline; n = 12 cells, 4 slices, 3 mice for TBS). Scale bars: 10 µm. (d) z-stack reconstruction of BDNFpro/GFP colocalization signals in astrocytes from basal- and TBS-slices from tamoxifen-treated p75-flox mice. Insets show GFP signal. BDNFpro/GFP colocalization was quantified using Mander's overlap. Data are normalized to baseline and presented as mean ± SEM. (n = 11 cells, 5 slices, 4 mice for baseline; n = 16 cells, 5 slices, 4 mice for TBS). Scale bar: 10 µm.

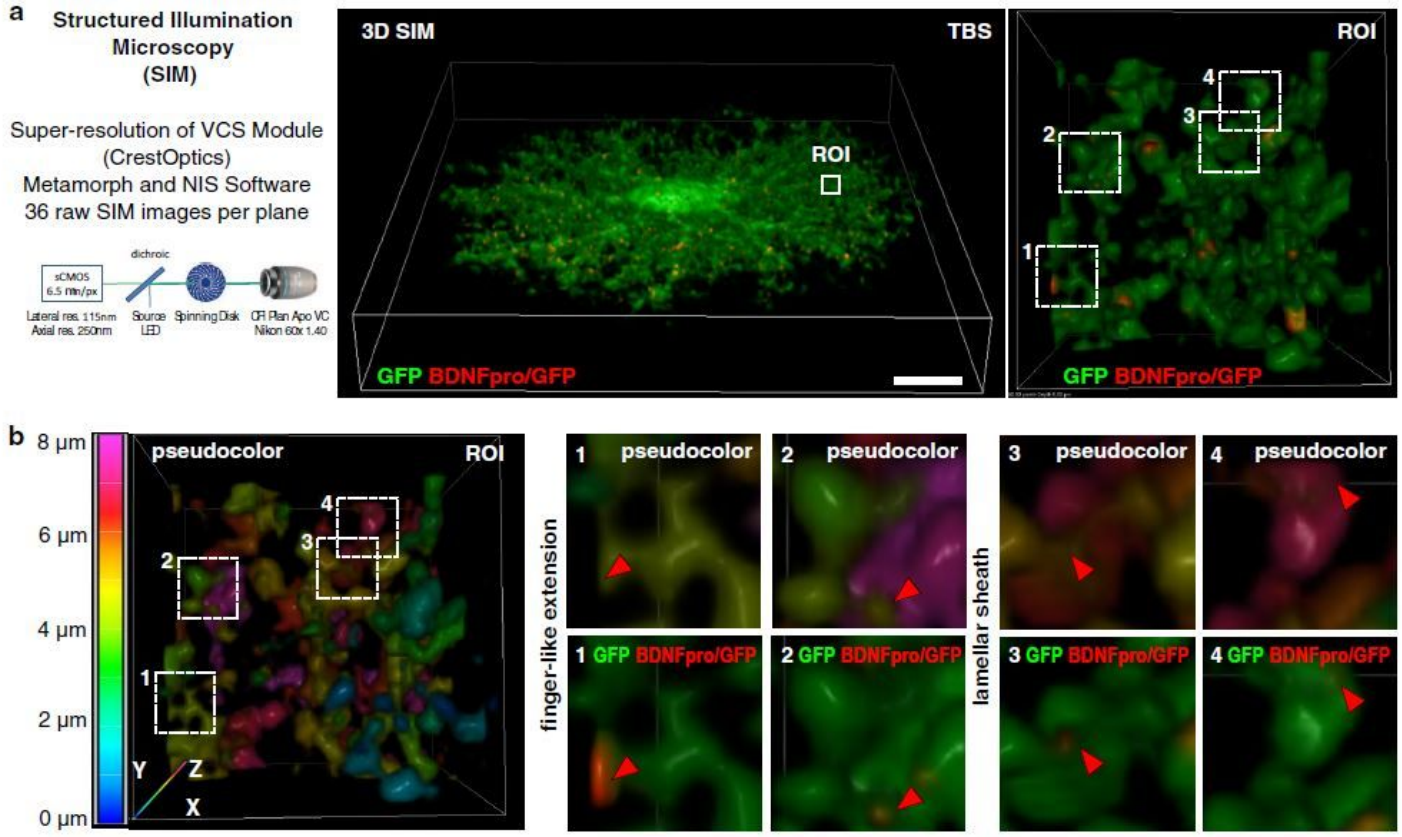

Figure 2

subcellular localization of BDNFpro (a) Graphical representation of the SIM super-resolution microscope (left). 3D-SIM image of a GFP-labeled astrocyte in a TBS-slice from control mice (middle). Twenty times magnification of a ROI shows BDNFpro/GFP colocalization signal localized in fine membrane extensions of the cell periphery (right). Scale bar: 10 µm. (b) 3D-SIM image of the ROI in (a); z-axe is visualized in pseudocolor to facilitate microdomains identification. Three times magnification of microdomains

characterized by the typical fingerlike extension (dashed squares 1 and 2) and flat lamellar sheath (dashed squares 3 and 4) are shown. BDNFpro/GFP colocalization is indicated (red arrowheads).

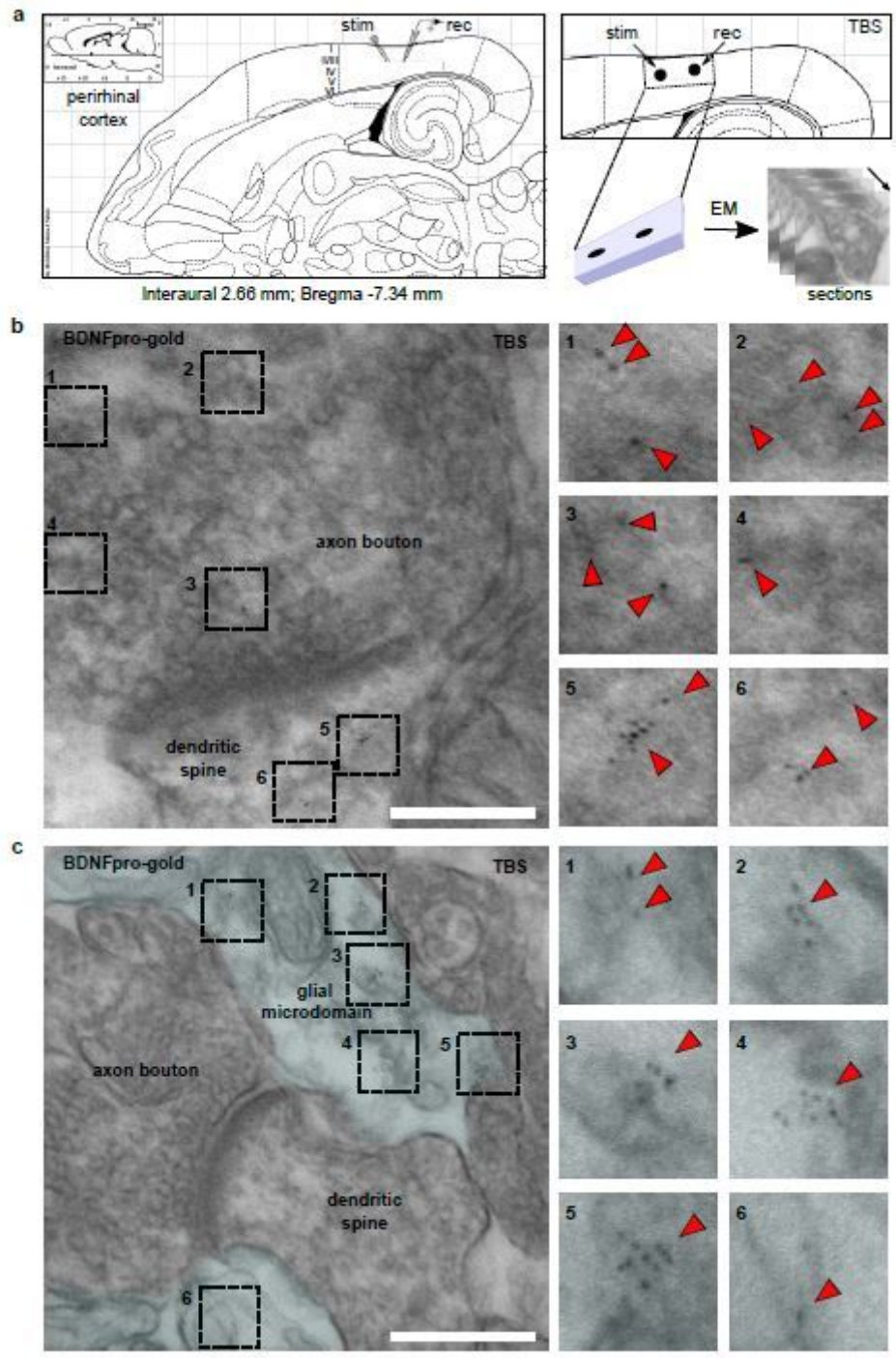

Figure 3

localization of BDNFpro in astrocytic microdomains (a) Experimental design linking field-potential with electron microscopy (EM) in layer II/III perirhinal cortex. TBS (10 min)-slices were dissected for EM processing. (b) Representative EM-image depicts BDNFpro-gold particles at axon bouton (dashed squares 1 to 4) and dendritic spine (dashed squares 5 and 6) (left). Three times magnification indicates

representative areas (dashed square 1 to 6) in which gold particles (red arrowheads) localization is shown (right). Scale bar: 100 nm. (c) Representative EM-image depicts BDNFpro-gold particles (dashed square 1 to 6) at astrocytic microdomains (light blue) (left). Three times magnification indicates representative areas (dashed square 1 to 6) in which gold particles (red arrowheads) localization is shown (right). Scale bar: 250 nm.

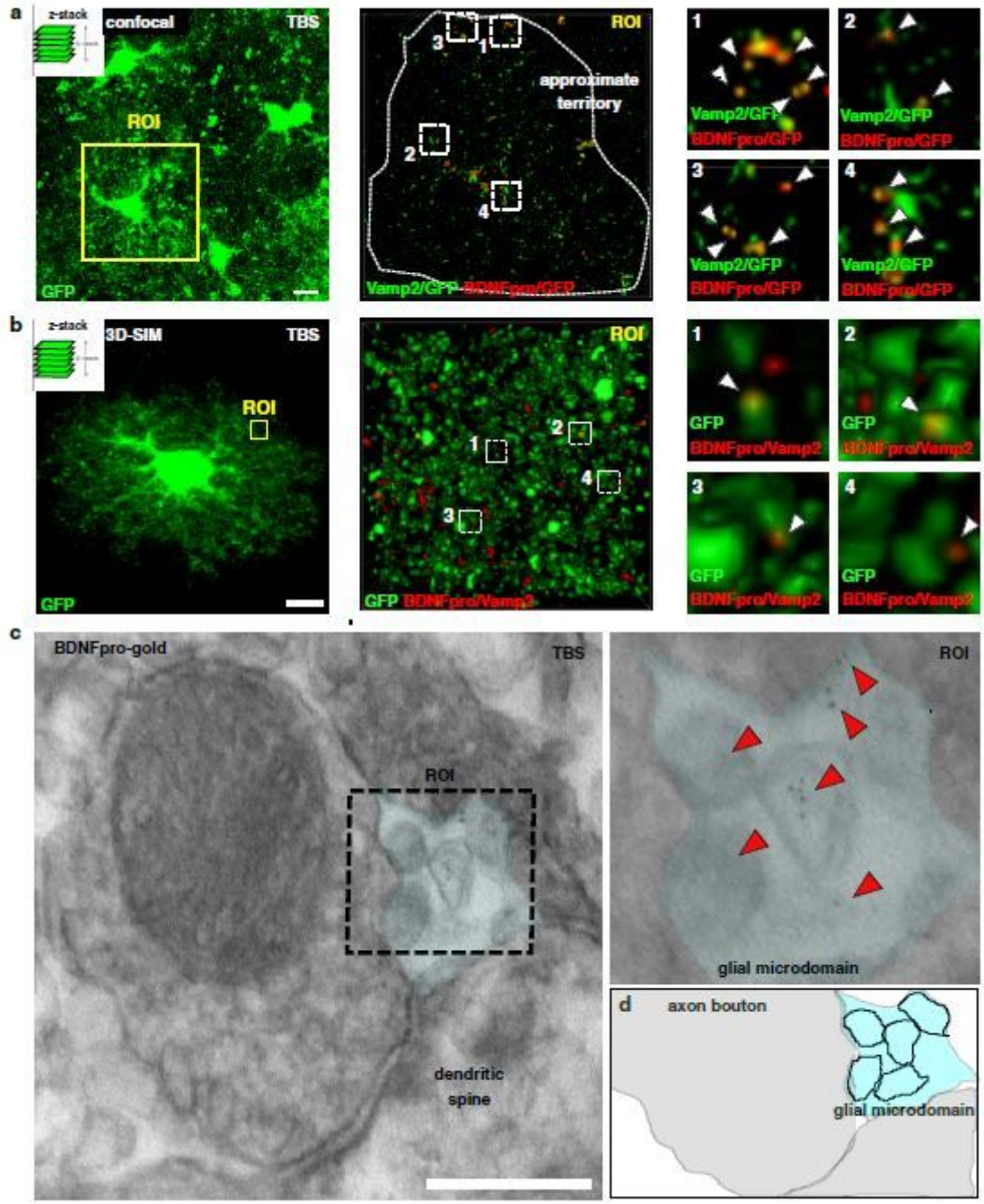

Figure 4

vesicular localization of BDNFpro (a) z-stack reconstruction shows astrocytes labeled by GFP (left). Cortical slices from control mice injected with AAV-GFAP-GFP virus were fixed 10 min after TBS and

processed for immunostaining and confocal analysis. Three times magnification of a ROI shows one GFP-astrocyte delimited by an approximate territory (white dashed) (middle). BDNFpro/GFP and Vamp2/GFP co-localizations signals are shown. Seven times magnification shows representative areas (dashed square 1 to 4) in which BDNFpro/GFP and Vamp2/GFP signals overlap (right). Scale bars: 5 μm. (b) 3D-SIM image of a GFP-labeled astrocyte in a TBS-slice from control mice (left). Twenty times magnification of a ROI (middle) in which BDNFpro/Vamp2 colocalization signal is shown. Seven times magnification shows BDNFpro/Vamp2 colocalization signal in fine membrane extensions of the cell periphery (dashed square 1 to 4) (right). Scale bar: 5 μm. (c) EM image depicts BDNFpro-gold at astrocytic microdomains (light blue) surrounding an axon bouton (left). Three times magnification of the ROI shows gold particles (red arrowheads) in vesicular-like structures (right). Scale bar: 100 nm. (d) Digital reconstruction of the image in (c). Astrocytic vesicles (black boundary) are shown. Scale bar: 100 nm.

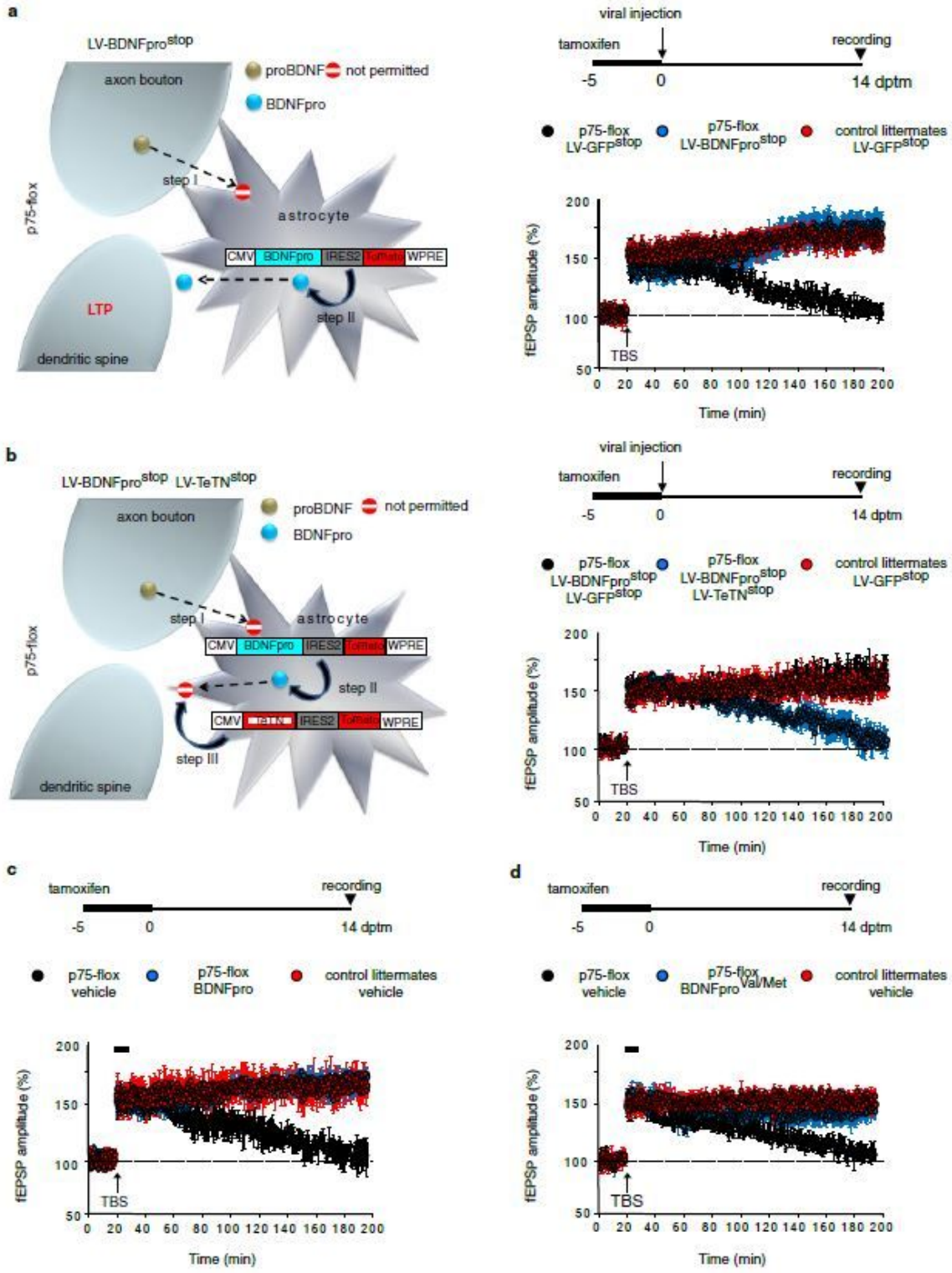

Figure 5

astrocytic BDNFpro secretion rescues LTP deficit in p75-flox mice (a) Schematic representation of the experimental design (left). Step I, deletion of p75NTR in astrocytes from tamoxifen-treated p75-flox mice precludes proBDNF transfer from neurons to astrocyte following TBS. Step II, LV-BDNFprostop transduction replaces BDNFpro in astrocytes. Schematic representation of the experimental paradigms (right); mice were treated with tamoxifen (-5 to 0), injected with lentiviruses the last day of tamoxifen

treatment (0 dptm) and finally recorded (14 dptm). LTP evoked in slices from p75-flox mice and control littermates injected with LV-GFPstop or LV-BDNFprostop is shown. Data are presented as mean ± SEM; (n = 10 slices, 6 mice for p75-flox/LV-GFPstop; n = 9 slices, 6 mice for p75-flox/LV-BDNFprostop; n=6 slices, 4 mice for control littermates/LV-GFPstop). (b) Schematic representation of the experimental design (left). Step II, and I as in (a). Step III, LV-TeTNstop transduction in astrocytes prevents from BDNFpro release. Schematic representation of the experimental paradigm as in (a) (right). LTP evoked in slices from p75-flox mice and control littermates injected with LV-GFPstop or co-injected with LV-GFPstop/LV-BDNFprostop and LV-TeTNstop/LV-BDNFprostop is shown. Data are presented as mean ± SEM; (n = 8 slices, 6 mice for p75-flox/LV-BDNFprostop/LV-GFPstop; n = 9 slices, 7 mice for p75-flox/LV-TeTNstop/LV-BDNFprostop; n=7 slices, 4 mice control littermates/LV-GFPstop). (c) LTP evoked in slices from p75-flox mice and control littermates. Mice were treated with tamoxifen (-5 to 0) and recorded 14 dptm. Slices were perfused (18-28 min) with vehicle or exogenous BDNFpro. Data are presented as mean ± SEM; (n=8 slices, 4 mice for p75-flox/vehicle; n=7 slices, 5 mice for p75-flox/BDNFpro; n=7 slices, 5 mice for control littermates/vehicle). (d) LTP evoked as in (c). Slices were perfused (18-28 min) with vehicle or BDNFproVal66Met. Data are presented as mean ± SEM; (n = 8 slices, 5 mice for p75-flox/vehicle; n = 6 slices, 4 mice for p75-flox/BDNFproVal66Met; n=7 slices, 5 mice for control littermates/vehicle).

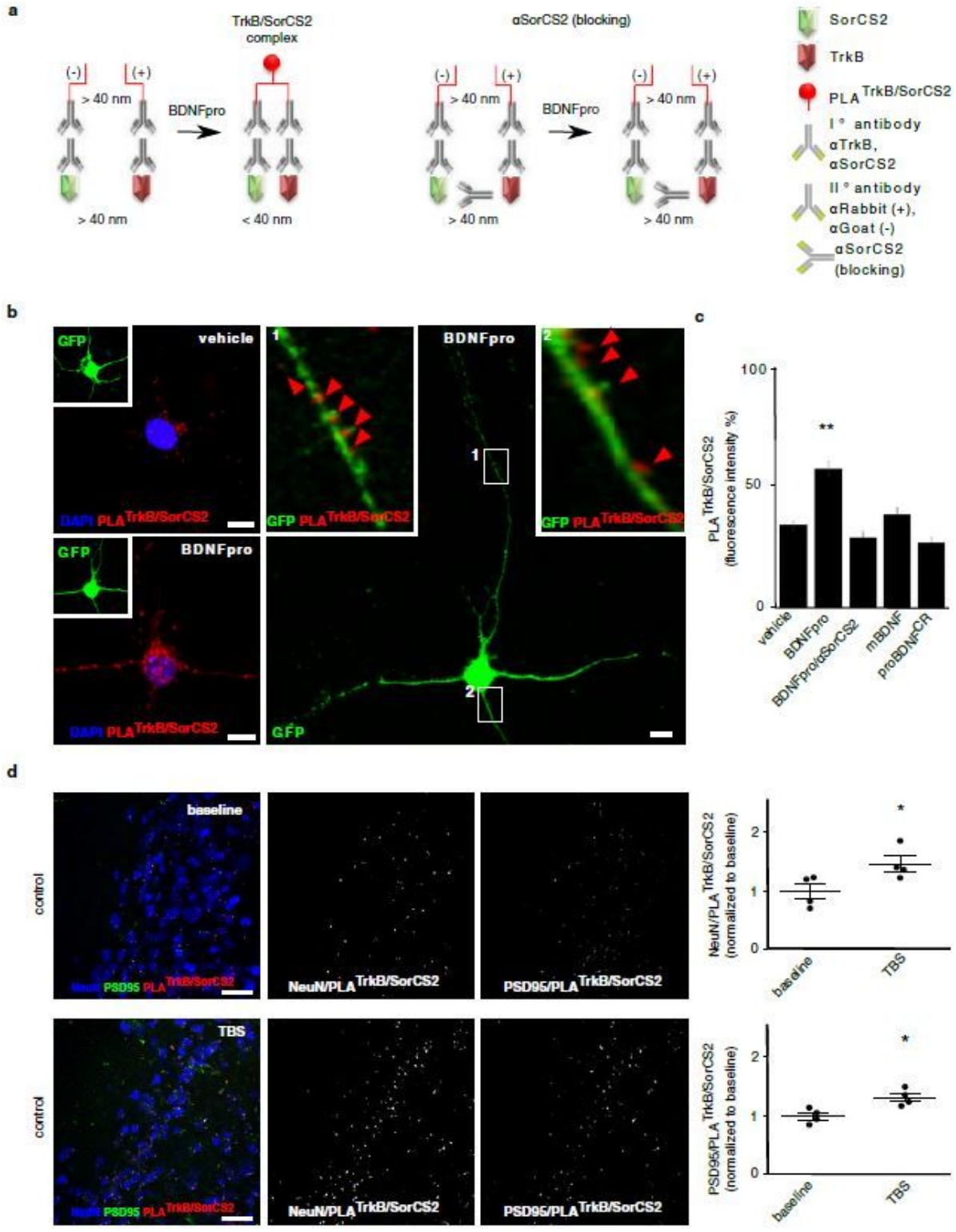

Figure 6

post-synaptic targeting of TrkB/SorCS2 complex (a) Schematic representation of the experimental design. Circular DNA probes (-) and (+) are coupled to II° antibody targeting αSorCS2 and αTrkB I° antibody. BDNFpro induces TrkB/SorCS2 complex formation (PLATrkB/SorCS2) that is prevented in the presence of αSorCS2 (blocking) antibody. (b) Left panel shows PLATrkB/SorCS2 signals in primary culture of cortical neurons treated with vehicle (upper) or BDNFpro (lower). The insets show reference

GFP-neurons. Right panel shows a GFP-neuron treated with BDNFpro. Five times magnification of regions of interest 1 and 2 shows dendritic PLATrkB/SorCS2 localization (red arrowheads). Scale bars: 5 µm. (c) Quantification of PLATrkB/SorCS2 signal in cultured neurons treated with vehicle, BDNFpro (in presence or absence of αSorCS2), mBDNF or proBDNFCR. Data are presented as mean ± SEM; ** $p<0.01$ (Unpaired t-test); (n = 111 cells, 3 cultures for vehicle; n=152 cells, 4 cultures for BDNFpro; n = 98 cells, 3 cultures for BDNFpro/aSorCS2; n = 89 cells, 3 cultures for mBDNF; n = 79 cells, 3 cultures for proBDNFCR). (d) z-stack reconstruction (left) showing NeuN, PSD95 and PLATrkB/SorCS2 signals in baseline (upper) and TBS (lower) slices. NeuN/PLATrkB/SorCS2 (center) and PSD95/PLATrkB/SorCS2 (right) colocalization signal is shown. Scale bars: 40 mm. NeuN/PLATrkB/SorCS2 and PSD95/PLATrkB/SorCS2 colocalization was quantified using Mander's overlap. Data are normalized to baseline and presented as mean ± SEM; * $p<0.05$ (Unpaired t-test); (n = 4 slices, 3 mice for each experimental condition).

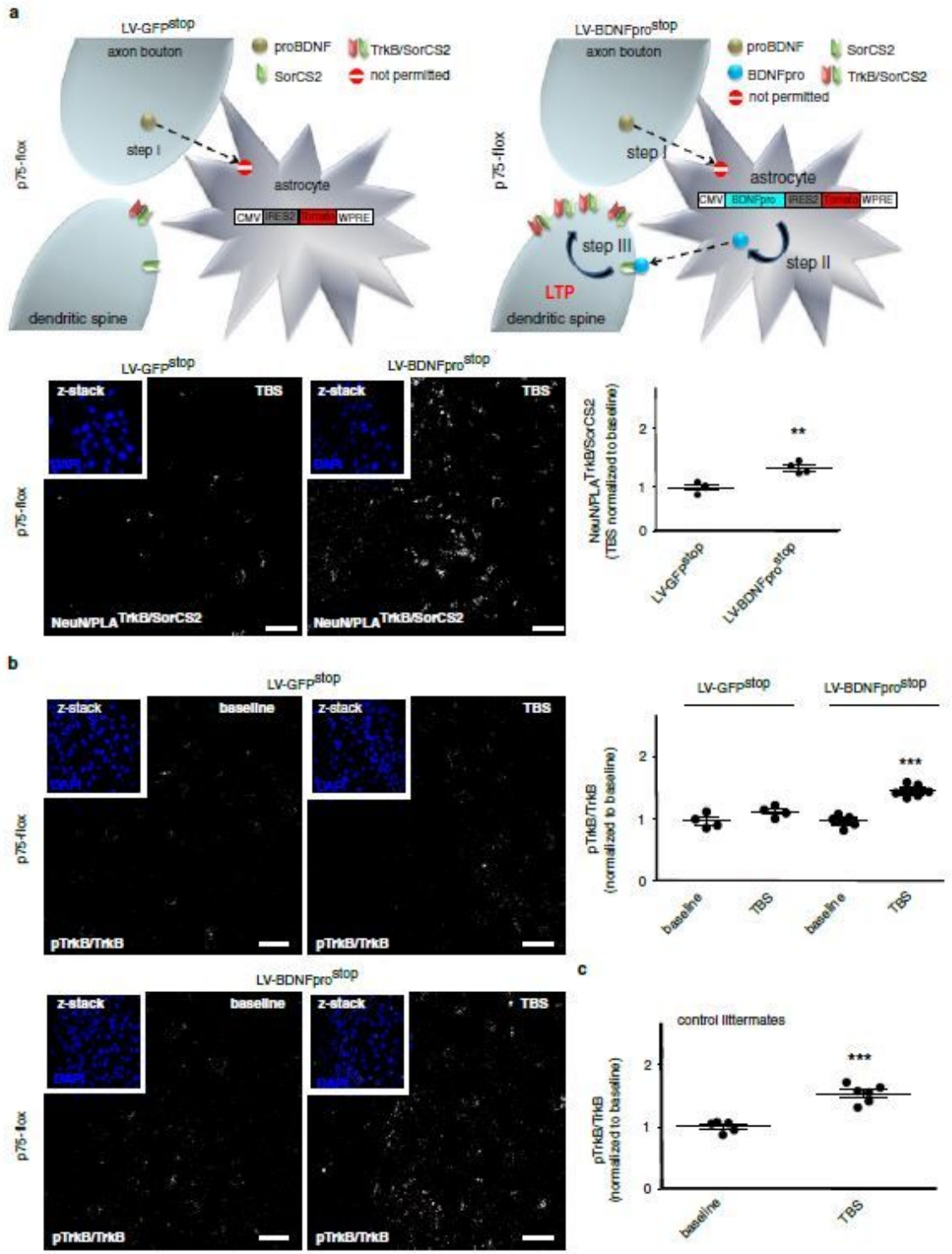

Figure 7

BDNFpro- induced TrkB/SorCS2 targeting and TrkB phosphorylation (a) Schematic representation of the experimental design (upper). Step I, deletion of p75NTR in astrocytes from tamoxifen-treated p75-flox mice precludes proBDNF transfer from neurons to astrocyte following TBS. Step II, LV-BDNFprostop transduction replaces BDNFpro in astrocytes. Step III, astrocytic BDNFpro provides final increase of TrkB/SorCS2 complexes in dendritic spines and LTP maintenance. z- stack reconstruction showing

NeuN/PLATrkB/SorCS2 colocalization signal in TBS-slices transduced with LV-GFPstop or LV-BDNFprostop (lower). The insets show field of analysis. NeuN/PLATrkB/SorCS2 colocalization was quantified using Mander's overlap. Data are normalized to baseline and presented as mean ± SEM; ** p<0.01 (Unpaired t-test); (n = 4 slices, 3 mice for each experimental condition). Scale bars: 40 µm (b) z-stack reconstruction showing pTrkB/TrkB colocalization signal in baseline- and TBS-slices from p75-flox mice transduced with LV-GFPstop (upper) or LV-BDNFprostop (lower). The insets show field of analysis. pTrkB/TrkB colocalization was quantified using Mander's overlap. Data are normalized to baseline and presented as mean ± SEM; *** p<0.001 (Unpaired t-test); (n = 4 slices, 3 mice for p75-flox mice/LV-GFPstop/TBS; n= 4 slices, 3 mice for p75-flox mice/LV-GFPstop/baseline; n = 6 slices, 4 mice for p75-flox mice/LV-BDNFprostop/TBS; n = 6 slices, 4 mice for p75-flox mice/LV-BDNFprostop/baseline). Scale bars: 40 µm. (c) Quantification of pTrkB/TrkB colocalization in baseline- and TBS-slices from control littermates using Mander's overlap. Data are normalized to baseline and presented as mean ± SEM; *** p<0.001 (Unpaired t-test); (n= 5 slices, 3 mice for control littermates/TBS; n= 6 slices, 3 mice for control littermates/baseline).

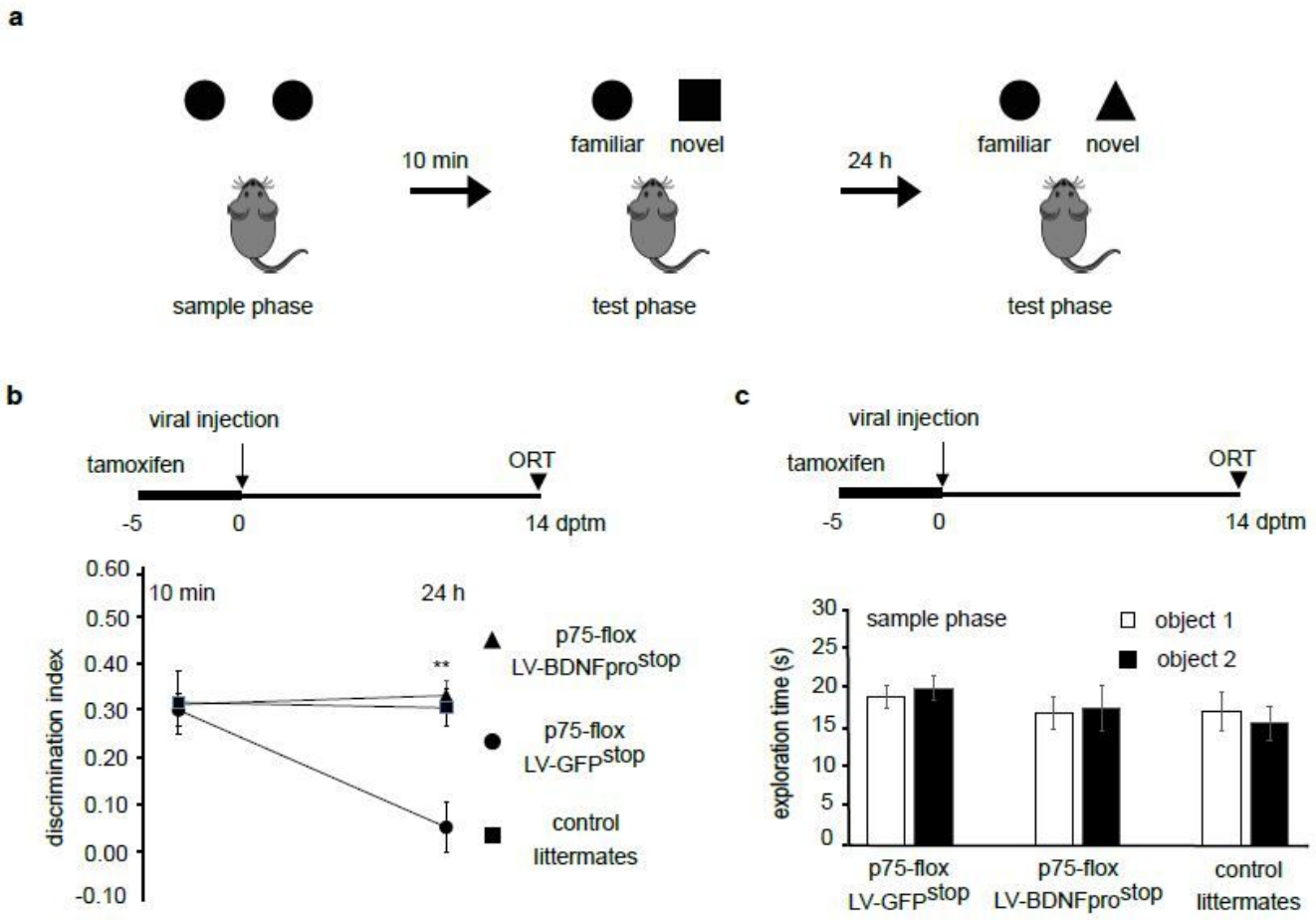

Figure 8

BDNFpro restores memory retention in p75-flox mice (a) Schematic diagram depicting the behavioral paradigm used for ORT. Mice were subjected to familiarization (sample phase) with two identical objects (circles). A test phase in which one familiar object (circle) is substituted with a novel one was performed after 10 min (square) and 24 h (triangle). (b) Schematic diagram depicting the experimental paradigm (upper). p75-flox mice and control littermates treated with tamoxifen (-5 to 0) and injected with LV-GFPstop or LV-BDNFprostop the last day of tamoxifen treatment (0 dptm) were subjected to ORT (14 dptm). Discrimination index is plotted against time interval between sample phase and test phases. Data are presented as mean ± SEM; ** $p<0.01$ (post hoc Holm-Sidak); (n = 11 mice for p75-flox/LV-GFPstop; n = 10 mice for p75-flox/LV-BDNFprostop; n= 5 mice for control littermates). (c) Schematic diagram depicting the experimental paradigm as in (b). The histogram shows mean exploration time of the familiar object and the novel object in the sample phase. Data are presented as mean ± SEM; (n = 11 mice for p75-flox/LV-GFPstop; n = 10 mice for p75-flox/LV-BDNFprostop; n= 5 mice for control littermates).

Supplementary Files

This is a list of supplementary files associated with this preprint. Click to download.

- Supplementaryfiguresandlegends.pdf